OXFORD

Cerebral Cortex, 2024, **34**, 1–21
https://doi.org/10.1093/cercor/bhad437
Advance access publication date 29 November 2023
Original Article

Hemispheric lateralization of language processing: insights from network-based symptom mapping and patient subgroups

Zhiyun Dai[1,†], Luping Song[2,†], Chongjing Luo[1], Di Liu[1], Mingyang Li[3], Zaizhu Han[1,*]

[1]State Key Laboratory of Cognitive Neuroscience and Learning & IDG/McGovern Institute for Brain Research, Beijing Normal University, Beijing 100875, China,
[2]Shenzhen Sixth People's Hospital (Nanshan Hospital), Huazhong University of Science and Technology Union Shenzhen Hospital, Shenzhen 518052, China,
[3]Key Laboratory for Biomedical Engineering of Ministry of Education, Department of Biomedical Engineering, College of Biomedical Engineering & Instrument Science, Zhejiang University, Yuquan Campus, Hangzhou 310027, China

*Corresponding author: State Key Laboratory of Cognitive Neuroscience and Learning & IDG/McGovern Institute for Brain Research, Beijing Normal University, Beijing 100875, China. Email: zzhhan@bnu.edu.cn

†Zhiyun Dai and Luping Song contributed equally to this work.

The hemispheric laterality of language processing has become a hot topic in modern neuroscience. Although most previous studies have reported left-lateralized language processing, other studies found it to be bilateral. A previous neurocomputational model has proposed a unified framework to explain that the above discrepancy might be from healthy and patient individuals. This model posits an initial symmetry but imbalanced capacity in language processing for healthy individuals, with this imbalance contributing to language recovery disparities following different hemispheric injuries. The present study investigated this model by analyzing the lateralization patterns of language subnetworks across multiple attributes with a group of 99 patients (compared to nonlanguage processing) and examining the lateralization patterns of language subnetworks in subgroups with damage to different hemispheres. Subnetworks were identified using a whole-brain network-based lesion-symptom mapping method, and the lateralization index was quantitatively measured. We found that all the subnetworks in language processing were left-lateralized, while subnetworks in nonlanguage processing had different lateralization patterns. Moreover, diverse hemisphere-injury subgroups exhibited distinct language recovery effects. These findings provide robust support for the proposed neurocomputational model of language processing.

Key words: hemispheric lateralization; language processing; white matter network; NLSM.

Introduction

Functional lateralization or asymmetry has existed for a long time in the animal kingdom. The hunting preference in Paleozoic predators, which appeared ∼500 million years ago, is the earliest known laterality of behavior (Babcock and Robison 1989; Güntürkün et al. 2020). Since then, some other nonlanguage lateral functions have evolved, such as behavioral performance (e.g. handedness, eye dominance, and foot dominance), sensory perception (e.g. vision, smell, and tactile perception), and even cognition (e.g. vocal, emotional, and social recognition) (Babcock and Robison 1989; Spinozzi and Cacchiarelli 2000; Vallortigara and Rogers 2005; Yamazaki et al. 2007; Giljov et al. 2012; Ocklenburg, Ströckens, et al. 2013; Ströckens et al. 2013; Siniscalchi et al. 2016). The human brain is also lateralized (Corballis 2017), avoiding repetitive information processing and reducing cognitive competition, and allowing it to perform complex and diverse cognitive functions efficiently given its limited size and weight (Corballis 2017; Güntürkün et al. 2020; Rogers 2021). Language, as a recently evolved high-level cognitive function of the human brain, has become an importantly and hotly studied scientific issue in modern neuroscience due to its lateralization. Revealing language lateralization can provide a better understanding of our brain and its cognitive functions (Frost et al. 1999; Knecht et al. 2000; Szaflarski et al. 2002). Moreover, because atypical lateralization of language is associated with some common disorders (e.g. epilepsy and schizophrenia; Stewart et al. 2014; Ocklenburg et al. 2015), the evaluation of language lateralization has been widely used in clinical neurological settings (Abbott et al. 2010; Jones et al. 2011; Janecek et al. 2013).

Although the language lateralization pattern in healthy people has been found to be related to a variety of factors (e.g. age, gender, handedness, and gene), most people still showed typical left language lateralization in brain activation (Shaywitz et al. 1995; Crow et al. 1998; Pujol et al. 1999; Knecht et al. 2000; Szaflarski et al. 2002, 2006, 2012; Dehaene-Lambertz et al. 2003; Wallentin 2009; Perlaki et al. 2013; Ocklenburg et al. 2014). In patients, the measurement of language laterality was important in epilepsy and brain tumors before surgery, which could avoid postoperative language deficit as much as possible (Baxendale et al. 2008; Arora et al. 2009; Ellmore et al. 2010; Jones et al. 2011; Pillai and Zaca 2011; Partovi et al. 2012; Zacà et al. 2012; Janecek et al. 2013; Stewart et al. 2014). Furthermore, the atypical language lateralization might be a critical manifestation of schizophrenia (Sommer et al. 2001, 2003; Ocklenburg, Westerhausen, et al. 2013; Sun et al. 2017). For epilepsy patients, bilateral or right-lateral language representation was relatively more common (Stewart et al. 2014). The stronger preference for left-handedness, the stronger left-laterality for the seizure, and the earlier age of seizures might lead to the stronger right-laterality of language function in patients with temporal lobe epilepsy (Isaacs et al. 2006; Stewart et al. 2014). In brain tumor patients, the people with tumors in the right hemisphere showed stronger left-laterality in language tasks than those with tumors in the left hemisphere; what is more,

Received: February 26, 2023. **Revised:** October 27, 2023. **Accepted:** October 27, 2023

the patients with tumors in the left Broca's or Wernicke's area compared with healthy controls would present more right laterality in language processing (Pillai and Zaca 2011; Partovi et al. 2012). For schizophrenia, the nonhallucinating patients showed weaker left language lateralization compared with healthy people, and patients with auditory hallucinations showed a larger effect in language lateralization reduction than the nonhallucinating patients (Ocklenburg, Westerhausen, et al. 2013). In stroke patients, about half of them presented deficits in spoken language and auditory language tasks when the strokes occurred in the left hemisphere, while just about 10% of the patients were impaired in auditory language tasks when the strokes occurred in the right hemisphere (Gajardo-Vidal et al. 2018).

The language function, as a distinct human ability, may exhibit differences in brain laterality when compared to nonlanguage functions. To compare the lateral difference between language and nonlanguage functions in gray matter cortices and white matter connections, extensive research has been conducted on healthy and lesioned brains (Thierry and Price 2006; Butler et al. 2009; Han et al. 2013; Herbet et al. 2018; Chen et al. 2019, 2020; Schumacher et al. 2019; Sundqvist et al. 2020). For example, early studies reported that a patient with a left thalamic hemorrhage had impaired language function and misinterpreted words (Takahashi et al. 1992), while another patient with a right temporal lobe lesion had impaired nonlanguage function, and misunderstood environmental sounds and noises (Fujii et al. 1990). Further studies revealed that language processing was lateralized to the left hemisphere, while nonlanguage processing was bilateral or lateralized to the right hemisphere (Thierry and Price 2006; Dick et al. 2007; Rosazza et al. 2009; Schumacher et al. 2019). For instance, this lateral pattern appeared across the temporal lobes (Gleissner et al. 1998; Snowden et al. 2004; Butler et al. 2009; Mesulam et al. 2013; Gainotti 2015; Chen et al. 2019), frontal lobes (Floel et al. 2004; Herbet et al. 2018), and their white matter connections (James et al. 2015; Sundqvist et al. 2020). However, others found that the right hemisphere was also vital for several aspects of language processing (Lindell 2006; Hartwigsen and Siebner 2012; Lambon Ralph et al. 2017; Gajardo-Vidal et al. 2018), including word recognition, production, reading, and prosodic and pragmatic processing (Lindell 2006; Hartwigsen and Siebner 2012). For example, studies using transcranial magnetic stimulation discovered that the right hemisphere helps us recognize both unfamiliar and concrete words (Braet and Humphreys 2006; Papagno et al. 2009; Hartwigsen and Siebner 2012). Many studies have observed almost comparable bilateral activation during phonological, lexical-semantic, and sentence processing (Sekiyama et al. 2003; Bright et al. 2004; James and Gauthier 2004; Vigneau et al. 2011; Gajardo-Vidal et al. 2018). A study found that semantic retrieval activated more brain regions in the right hemisphere than in the left hemisphere, and the degree of activation of the right ventral lateral prefrontal cortex was significantly correlated with the semantic constraint level (Vartanian and Goel 2005). Another study found that Mandarin language learning ability scores of English speakers were significantly correlated with their prelearning diffusion tensor imaging measures in right fiber bundles (i.e. the right superior longitudinal fasciculus and the right inferior longitudinal fasciculus) but not left fiber bundles (Qi et al. 2015).

The above seemingly contradictory findings on language lateralization (left-lateral vs. bilateral) may be due to the language network difference between healthy and brain-damaged individuals (Chang and Lambon Ralph 2020). Some studies have found that language processing in healthy individuals appeared to be bilateral but more asymmetrical in the left hemisphere (Binder et al. 2000; Cogan et al. 2014; Poeppel 2014; Zacà et al. 2018), while previous studies showed that the language processing was strongly left-lateralized in patients. This phenomenon might suggest a difference in the left hemisphere which had more computational capacity in language processing than the right hemisphere. This difference was reflected more in the white matter rather than gray matter (Parker et al. 2005; Catani et al. 2007; Bain et al. 2019), potentially contributing to a higher risk of chronic impairment after the left than the right brain damage. A previous neurocomputational model has been proposed to accomplish a unified and comprehensive framework to explain different language lateralization in healthy and patient individuals (Chang and Lambon Ralph 2020). This model suggests that in healthy individuals, there is an initial discrepancy in language processing capacity between the left and right hemispheres, with the left hemisphere taking on more of the computational load, resulting bilateral but asymmetrical pattern in healthy people (Chang and Lambon Ralph 2020). In cases where the right hemisphere was damaged, the left hemisphere might compensate to restore the lost language function. Similarly, when the left hemisphere sustained mild damage, other regions within the left hemisphere and the right hemisphere could collaborate to restore language function. However, in situations of severe damage in the left hemisphere, the right hemisphere may not possess sufficient capacity to fully restore the lost language function (Chang and Lambon Ralph 2020). This compensatory effect might be attributed to two mentioned mechanistic frameworks for language recovery: degeneracy and variable neurodisplacement (Chang and Lambon Ralph 2020; Stefaniak et al. 2020). Regarding the degeneracy mechanism (Price and Friston 2002; Chang and Lambon Ralph 2020; Stefaniak et al. 2020), the language cognitive function might result from multiple neural networks with distinct structures, generating a partially adaptable system. When the brain was damaged, language recovery could be facilitated through the up-regulation of dormant regions, the utilization of alternative pathways, or the involvement of nonlanguage regions that were not typically recruited in the healthy state. Furthermore, the variable neurodisplacement mechanism emphasized the necessity to balance metabolic energy costs against performance demands (Attwell and Laughlin 2001; Chang and Lambon Ralph 2020). Therefore, when the language performance demand was not maximum, some regions of the language network could be down-regulated to conserve energy. When the performance demand was high or a part of the network was damaged, these down-regulated regions could be reactivated for use.

In our study, a group of 99 patients (most of them suffered from stroke) and a network-based lesion-symptom mapping (NLSM) method (Li, Song, et al. 2021) were used to investigate this neurocomputational model (Chang and Lambon Ralph 2020). The NLSM method was chosen as it offered advantages in measuring the whole-brain white matter connectome as opposed to isolated tracts. It allowed the selection of the subnetwork most relevant to each attribute from the whole-brain white matter structural network (Li, Song, et al. 2021). First, the white matter subnetworks for language processing in the whole group were measured to find out whether the language processing subnetworks in patients were consistently left-lateral. Subsequently, the whole group was divided into three subgroups (left-lesion, right-lesion, and bi-lesion subgroups) to investigate whether the impairment and recovery of language function were modulated by different hemisphere-damage patterns as described in the model. Given the two mechanism frameworks in consideration (Stefaniak et al. 2020), the laterality observed in each subnetwork

merely reflects the profile of that specific subnetwork rather than the entire language network. Therefore, our tasks involved a broader range of language processing components as much as possible. These tasks presented a sentence question related to a specific attribute (e.g. "Which one is brownish?") at the top, followed by two candidate object words (lion or penguin) at the bottom. This task necessitates multiple cognitive computations and representations, at least including visual input, orthographic recognition, syntactic encoding, semantic access, competitor inhibition, and accessing the correct answer (Cutting et al. 2006). Furthermore, we held six specific attribute tasks (form, color, motion, sound, manipulation, and function) in language processing, which could cover more language processing nodes. Previous studies also found different bilateral and left-lateral patterns in healthy people with five different attributes (form, color, motion, sound, and manipulation) (Fernandino, Binder, et al. 2016; Fernandino, Humphries, et al. 2016). These specific attributes referred to the aspects of conceptual knowledge closely related to the sensorimotor experiences of objects (e.g. form, color, motion, sound, and manipulation attributes) rather than sensory input channels (e.g. vision, hearing, and smell) (Hoffman and Lambon Ralph 2013; Fernandino, Binder, et al. 2016). To compare with our language subnetworks in the whole patient group, the nonlanguage subnetworks in these specific attributes were also measured. We anticipated that the nonlanguage subnetworks might be more bilateral or right-lateral. The lateralization pattern of each subnetwork was quantitatively assessed using the lateralization index (LI) from three profiles (nodes, edges, and network) of the subnetwork (Iturria-Medina et al. 2011; James et al. 2015; Li, Tang, et al. 2021).

Materials and methods

Participants

Ninety-nine patients with brain damage (78 males; ages: 44.37 ± 13.39 years old; formal education: 12.76 ± 3.36 years) were recruited from the China Rehabilitation Research Center. Participants did not have any brain injury until at least 1-month postonset, and most suffered from hemorrhage ($n = 30$), infarction ($n = 46$), or trauma ($n = 17$). No participants had other neurological or psychiatric conditions, such as alcoholism, schizophrenia, or depression. All were native Chinese speakers. Most ($n = 93$) were right-handed (Oldfield 1971) (see details in Table 1). Each patient provided informed written consent. This study was approved by the Institutional Review Board of the National Key Laboratory of Cognitive Neuroscience and Learning at Beijing Normal University.

A dataset of 51 healthy controls was also collected (27 males; ages: 49.94 ± 10.66 years old; formal education: 13.02 ± 3.85 years; see details in Supplementary Table 1) to evaluate the impairment degree of patients' behavioral performance and to achieve the task difference validation (details see as below).

Behavioral data collection and preprocessing

We evaluated patients' ability to process six attributes: form (i.e. the shape and tactility knowledge of objects), color (i.e. the typical color knowledge of the objects), motion (i.e. the visual movement pattern of objects), sound (i.e. the voice or sound of objects), manipulation (i.e. the knowledge about how objects can be physically interacted with using our hands), and function (i.e. the information regarding the use and purpose of objects). Each attribute was assessed in two tasks (a language task and a nonlanguage task). These tasks were adapted from those used in the literature (e.g. Riddoch and Humphreys 1993; Caramazza and Shelton 1998; Chen et al. 2020). They were an object attribute matching or verification two-alternative forced choice (2AFC) task. The subjects responded by selecting an option using the touch screen in the matching task or by pressing the "是" (Yes) or "否" (No) button in the verification task. The procedure was run by the DisplayMaster DirectX (DMDX) Windows-based program (Forster and Forster 2003). The tasks were individually performed in a quiet testing room. No session lasted longer than 2 h; brief breaks for rest were permitted as needed. The testing sequence of trials addressing each of six attributes in each task was pseudorandom, and identical across patients. Subjects were instructed to respond within 60 s. The first response for each trial was recorded as the subject's response.

Language task

The stimuli in each trial were visually presented on a touch screen in the Chinese language with a question regarding a specific attribute [e.g. 哪个是棕色的?" (Which one is brown?)] at the top of the screen and two candidate object words [e.g. "狮子" (lion) or "企鹅" (penguin)] at the bottom. The patients were instructed to select the correct answer from the two candidates for each question. The number of trials and an example of each attribute are given below.

Form matching ($n = 75$). "哪个是长方形的" (Which one is rectangular?), "手镯" (bracelet) or "相机" (camera);

Color matching ($n = 30$). "哪个是黑白相间的" (Which one is black-and-white?), "斑马" (zebra) or "袋鼠" (kangaroo);

Motion matching ($n = 30$). "哪个移动得更慢" (Which one moves more slowly?), "大象" (elephant) or "猎豹" (leopard);

Sound matching ($n = 45$). "谁的声音更大" (Whose sound is louder?), "蜗牛" (snail) or "老虎" (tiger);

Manipulation matching ($n = 30$). "哪一个能够单手使用" (Which one is manipulated with one hand?), "温度计" (thermometer) or "领带" (necktie);

Functional matching ($n = 60$). "哪一个通常用作食物" (Which one is used for food?), "玫瑰" (rose) or "芹菜" (celery).

Nonlanguage task

The stimuli were visual grayscale pictures of objects unless otherwise specified (e.g. a visual video or auditory sound). The number of trials and an example of each attribute are provided below.

Form verification ($n = 60$). Subjects were instructed to decide whether two object parts (e.g. the head of a squirrel and the body of a monkey) came from the same object.

Color verification ($n = 20$). Subjects were instructed to decide whether the color of a color patch (e.g. yellow patch) was common for an object (e.g. potato).

Motion verification ($n = 57$). Subjects were instructed to decide whether a point-light motion animation of an object (e.g. flying of a bird) was consistent with the action for an object (e.g. dog).

Sound verification ($n = 42$). Subjects were instructed to decide whether the sound of an object (e.g. the sound of a ring) heard via earphone was typically produced by an object (e.g. camera).

Manipulation matching ($n = 20$). Subjects were instructed to decide which of two objects (e.g. axe, match) presented at the bottom of the screen was more similarly manipulated to an object (e.g. hammer) at the top of the screen.

Functional matching ($n = 30$). Subjects were instructed to decide which of two objects (e.g. necklace, envelope) presented at the bottom of the screen was more similar in function to the object (bracelet) at the top of the screen.

For each attribute, we collected the participants' original responses and scored them for accuracy. Because our behavioral

Table 1. Demographics of the 99 patients.

Patient No.	Sex	Age (year)	Education (year)	Hand-edness	Cause of disease	Patient No.	Sex	Age (year)	Education (year)	Hand-edness	Cause of disease
1	F	19	12	R	TMA	51	M	42	12	R	Hem
2	F	22	16	R	Hem	52	M	42	14	R	Inf
3	F	25	12	R	TMA	53	M	43	15	R	Inf
4	F	26	9	R	Anoxic encephalopathy	54	M	43	16	R	Inf
5	F	35	12	R	Inf	55	M	43	19	R	Inf
6	F	35	15	L	Hem	56	M	45	9	R	TMA
7	F	37	9	R	TMA	57	M	45	12	R	Hem
8	F	37	12	R	Inf	58	M	45	15	R	Inf
9	F	39	15	R	Hem	59	M	45	16	R	Inf
10	F	40	12	R	TMA	60	M	46	9	R	Inf
11	F	40	15	R	Inf	61	M	46	12	R	Inf
12	F	41	15	R	Hem	62	M	46	16	R	Inf
13	F	45	9	R	TMA	63	M	47	9	R	Inf
14	F	45	15	R	Inf	64	M	47	12	R	TMA
15	F	51	8	R	Inf	65	M	47	12	R	Inf
16	F	52	6	R	Inf	66	M	47	15	R	Inf
17	F	56	12	R	Hem	67	M	47	16	R	Inf
18	F	56	12	R	Inf	68	M	47	16	R	Hem
19	F	64	12	R	Inf	69	M	48	9	R	Hem
20	F	70	16	R	TMA	70	M	48	15	R	Inf
21	F	76	2	R	thrombosis	71	M	48	15	R	Hem
22	M	19	12	R	TMA	72	M	48	19	R	Hem
23	M	20	9	mixed	TMA	73	M	49	12	R	Inf
24	M	20	9	R	Hem	74	M	49	15	R	Hem
25	M	20	15	R	TMA	75	M	49	16	R	Hem
26	M	21	12	R	TMA	76	M	51	9	R	Inf
27	M	22	12	R	TMA	77	M	51	15	R	Cerebrovascular disorder
28	M	22	15	R	TMA	78	M	52	12	R	Inf
29	M	24	9	R	TMA	79	M	53	12	R	Inf
30	M	26	16	R	Inf	80	M	54	16	R	Inf
31	M	28	16	R	Inf	81	M	55	15	R	Inf
32	M	28	16	R	Hem	82	M	55	15	R	Hem
33	M	30	12	L	TMA	83	M	56	2	R	Inf
34	M	30	19	R	Inf	84	M	56	15	R	Inf
35	M	32	12	R	electric shock	85	M	57	6	R	Inf
36	M	32	15	R	Hem	86	M	58	9	R	Inf
37	M	34	12	R	Hem	87	M	58	12	R	Inf
38	M	35	16	R	Inf	88	M	58	15	R	Inf
39	M	35	16	R	Inf	89	M	59	4	R	delayed encephalopathy
40	M	36	15	R	Hem	90	M	60	16	R	Hem
41	M	36	16	L	Hem	91	M	60	16	L	Inf
42	M	37	12	R	Inf	92	M	61	15	R	Hem
43	M	39	12	L	Hem	93	M	62	12	R	Inf
44	M	40	8	R	TMA	94	M	63	12	R	Inf
45	M	40	12	R	Hem	95	M	65	9	R	Inf
46	M	40	15	R	Hem	96	M	67	9	R	Inf
47	M	40	16	R	Hem	97	M	67	12	R	Thrombosis
48	M	40	16	R	Hem	98	M	70	12	R	Inf
49	M	41	9	R	Hem	99	M	74	12	R	Hem
50	M	41	15	R	Hem						

Note. F = female; M = male; L = left-handed; R = right-handed; TMA = trauma; Hem = hemorrhage; Inf = infarction.

tasks contained different item numbers, comparing patients' performance by raw scores might not be appropriate. To address this, a normalization process for raw scores within each task was performed among the patient group. We calculated the z score by the following formula:

$$z = \frac{X - \mu}{\sigma},$$

where X is the raw data, μ and σ are the mean value and standard deviation (SD) of the group in each task. These z-scores were used in the following analyses.

Imaging data collection and preprocessing

Patients were scanned at the China Rehabilitation Research Centre using an 8-channel split head coli 1.5 T GE SIGNA EXCITE

scanner. Three types of images were collected: (i) T_1-weighted 3D gradient echo images with magnetization-prepared rapid gradient echo acquisition, (ii) T_2-weighted fluid attenuated inversion recovery images, and (iii) diffusion-weighted images (DWI). The T_1 images were collected in the sagittal plane using the following parameters: a matrix size of 512×512, field of view (FOV) of 250×250 mm^2, voxel size of $0.49 \times 0.49 \times 0.70$ mm^3, repetition time (TR) of 12.26 ms, echo time (TE) of 4.2 ms, inversion time of 400 ms, flip angle of 15°, and 248 slices. Two identical sequences of T_1 images were acquired, and the average of the images was used to increase the signal-to-noise ratio in our analyses. The T_2 images were used as a visual reference for manually drawing precise lesion contours on the T_1 images. They were collected in the axial plane with the following parameters: a matrix size of 512×512, FOV of 250×250 mm^2, voxel size of $0.49 \times 0.49 \times 5$ mm^3, TR of 8002 ms, TE of 129.57 ms, inversion time of 2 s, flip angle of 90°, and 28 slices. Two DWI sequences in different directions ($n = 15$ and 17) were collected to increase the direction number. Each sequence adopted the following parameters: a matrix size of 128×128, FOV of 250×250 mm^2, voxel size of $1.95 \times 1.95 \times 2.6$ mm^3, TR of 13,000 ms, TE of 69.3 ms, inversion time of 0 s, flip angle of 90°, and 53 slices. The first two volumes were b_0 volumes, and the b-value of other volumes was 1000 s/mm^2 in each sequence. We scanned twice of the T_1 and DWI images to improve their quality.

Using MATLAB software, images of each patient were preprocessed with the following main steps (Han et al. 2013). (i) Each of the two T_1 images was coregistered to the same native space using the trilinear interpolation method, and then, images were averaged using Statistical Parametric Mapping (SPM5) software (https://www.fil.ion.ucl.ac.uk/spm/). (ii) The T_2 images were coregistered and resliced to align with the averaged T_1 images. Two skilled individuals (Chen J and Feng T) visually drew the lesion contours on the average T_1 images slice-by-slice, referring to the T_2 images as needed. (iii) The T_1 images were normalized into Talairach space in BrainVoyager QX v2.0 (Goebel 2012) and the Advanced Normalization Tools (ANTs) software package (Tustison et al. 2014). We used BrainVoyager QX v2.0 (www.brainvoyager.com) to accurately and manually delineate each patient's lesion contour. Because this software was based on neuroimages in the Talairach space, we utilized the ANTs (http://www.picsl.upenn.edu/ANTS/) software package to extract the affine transformation matrix between the native and Talairach spaces. (iv) This transformation matrix was then employed to register and transform the lesion description into the Talairach space using the "WarpImageMultiTransform" program, and the T_1 images were further transformed into the Montreal Neurological Institute (MNI) space. (v) The two DWI sequences were combined into one single nifty-1 format file, and then, the diffusion-weighted gradient tables of the two sequences were combined. (vi) The DWIs were further processed with the following stages using the pipeline for analyzing brain diffusion images (Cui et al. 2013), which entailed used of Brain Extraction Tool (BET) function to remove the skull, the Eddycorrect function to correct eddy current distortions, and the Diffusion Tensor Imaging Fit command to fit a diffusion tensor model at each voxel and build diffusion tensor models. Executing BET produced fractional anisotropy (FA) maps in the individual space, which were registered using ANTs (version 1.9) with the functional magnetic resonance imaging of the brain FA template in the MNI space. The FA maps were then normalized with a linear rigid affine and nonlinear transform registration.

NLSM analysis

The NLSM method (Li, Song, et al. 2021) was applied to determine the optimal white matter subnetwork underlying the processing of each attribute from the whole-brain network. It included the following main steps (Li, Song, et al. 2021).

Construction of the whole-brain white matter network of each patient

Since brain damage in patients often led to abnormal diffusion signals, we chose an approach based on the healthy population atlas to mitigate data quality issues (Oishi et al. 2009; Preti et al. 2012; Lin et al. 2015; Gleichgerrcht et al. 2017; Schilling et al. 2019). A white matter connectome atlas in MNI space was extracted from data of 842 healthy people in the Human Connectome Project (Yeh et al. 2018; Griffis et al. 2020). For each patient, we first identified the spared fibers in the healthy atlas, which bypassed the brain lesion mask of the patient using DSI studio software. Then, a spared network was reconstructed by extracting the spared fibers between each pair of 90 gray matter regions in the Automated Anatomical Labeling atlas (AAL90 without the cerebellum, Tzourio-Mazoyer et al. 2002; Zou et al. 2018). Finally, the FA network was created by masking all fibers in each pair of regions that had spared fibers and calculating the mean FA value in the tract mask (i.e. averaged FA values based on the DWI data of each voxel of the mask per patient). The FA value of a tract connecting the two regions reflected the white matter connectivity strength of that tract. As a result, a whole-brain FA network containing 90 regions (i.e. a 90 × 90 matrix) was obtained for each patient.

Identification of the subnetworks underlying each attribute processing in language and nonlanguage tasks

The whole-brain FA network (90 × 90 nodes) could be divided into $\sim 1.24 \times 10^{27}$ subnetworks (containing between 2 and 90 nodes). The purpose of this analysis was to identify the subnetwork with the information exchange ability that could best explain the behavioral variation (S_{bhv}) among the 99 patients processing each attribute in language or nonlanguage tasks. Here, the global efficiency (E^w) of each subnetwork here was treated as the index of information exchange ability for subnetwork (Latora and Marchiori 2001), which was calculated using the following formula (Latora and Marchiori 2001; Rubinov and Sporns 2010):

$$E^{\mathrm{W}} = \frac{1}{n} \sum_{\mathrm{i} \in N} \frac{\sum_{j \in N, j \neq \mathrm{i}} \left(d_{ij}^{w}\right)^{-1}}{n-1},$$

where N is the set of regions in the subnetwork, n is the number of regions, and d_{ij}^{w} is the weighted shortest path length between regions i and j (Rubinov and Sporns 2010). Thus, the objective function of the relationship between S_{bhv} and E^w for a given subnetwork in the patients could be expressed in the following regression equation:

$$S_{bhv} = \alpha \cdot E^{\mathrm{W}} + \beta + \varepsilon,$$

where α and β are the regression coefficients, and ε is the error term.

To quantitatively measure the relationship between S_{bhv} and E^w, we further calculated the explanatory power (R^2) of E^w with

regard to S_{bhv} for each subnetwork using the following equation:

$$R^2 = 1 - \frac{\sum_{i=1}^{n_{sub}} (y_i - f_i)^2}{\sum_{i=1}^{n_{sub}} (y_i - \bar{y})^2},$$

where y_i is an observed value (behavioral scores), $\bar{y}$ is the mean value of all y_i, f_i is the predicted behavioral value corresponding to the minimum ε value in the previous equation, and n_{sub} is the number of all patients. Thus, an R^2 value could be calculated for each subnetwork. A higher R^2 corresponded to a higher explanatory power of the subnetwork for behavioral scores. Therefore, we attempted to find the subnetwork with the maximum R^2 value among all 1.24×10^{27} subnetworks for each attribute behavior.

The number of potential subnetworks for the whole-brain network was too large to be exhaustively examined under the present conditions. To reduce the computation time, we adopted a genetic algorithm (GA; Goldberg 1989), which was able to obtain approximate results in less computation time.

Ultimately, we obtained the optimal subnetwork underlying processing of each of the six attributes in language or nonlanguage tasks, having the highest R^2 value, and the most explanatory power for the attribute scores. We obtained 12 attribute-relevant subnetworks corresponding to the processing of the six attributes in each of the language and nonlanguage tasks. For all optimal subnetworks, we implemented the false discovery rate (FDR) correction (Benjamini and Hochberg 1995; Benjamini and Yekutieli 2001, 2005).

Subnetwork lateralization measurement

To investigate the lateralization of each attribute-relevant subnetwork obtained by the above analyses, we calculated the LI of the subnetwork using the formula:

$$LI = \frac{(\sum X_{left} - \sum X_{right})}{(\sum X_{left} + \sum X_{right})},$$

where X_{left} and X_{right} are the values of a given index in the left and right hemispheres within the subnetwork, respectively (Wilke and Lidzba 2007). We investigated three indices: the node number, edge number, and sum of nodal degrees of the subnetwork (Iturria-Medina et al. 2011; James et al. 2015; Li, Tang, et al. 2021). The nodal degree (k_i) of each node was used to reflect how well a node is connected in the network and computed using the following formula (Rubinov and Sporns 2010; Zhao et al. 2017):

$$k_i = \sum_{i,j \in N} a_{ij},$$

where i, j are the nodes and a_{ij} is the connection coefficient between i and j.

The LI value ranges from −1 to +1. Following previous criteria (Briellmann et al. 2006; Wilke and Lidzba 2007), LI values <−0.20, −0.20–0.20, or >0.20 reflected right-lateralized, bilateral-, or left-lateralized subnetworks, respectively.

Validation of the subnetworks

To determine whether each attribute subnetwork obtained from the above analyses was reliable, we further performed the four following validation analyses: examining whether each subnetwork had the issues of task differences, random chance, overfitting, or method problems.

The task difference problem

The processing ability of each of the six attributes was tested using a 2AFC paradigm regardless of whether the task was a language and or nonlanguage task. Subjects' response method was different between language and nonlanguage tasks (matching vs. verification) for four of the attributes. Therefore, asymmetric differences among the 12 attribute-relevant subnetworks might arise from task differences instead of cognitive differences. To test this possibility, each raw accuracy of each patient was normalized as a t value using data from 51 healthy controls (Crawford and Garthwaite 2006; Han et al. 2013; Chen et al. 2020). The corrected t value reflected the degree of severity of deficits in the attribute and may resolve the task difference problem to some extent (see details of this method in Crawford and Garthwaite 2006; Han et al. 2013). In summary, for each task, we initially established a regression model using data from the healthy control group. The model employed accuracy scores as the dependent variable and included predictors such as age, gender, and years of formal education. By integrating each patient's demographic information into the model, we derived a predicted accuracy score, which enabled us to calculate a discrepancy value ($\text{Discrepancy}_{\text{patient}}$) by contrasting observed accuracy with predicted accuracy. Subsequently, we calculated a corrected standard error of estimate ($\text{SE}_{\text{patient}}$) for each patient. The patient's t-score was then computed using the formula:

$$t - \text{score}_{\text{patient}} = \frac{\text{Discrepancy}_{\text{patient}}}{\text{SE}_{\text{patient}}}.$$

Therefore, the NLSM analysis was repeated using the corrected t-scores as behavioral scores. We compared the structure and LI values between the original and new subnetworks for each attribute.

The random chance problem

A permutation test was used to inspect whether each subnetwork was obtained by random chance. We repeated the NLSM analysis as described above, except that the behavioral scores of the 99 patients were randomly paired with another patient's brain images. These R^2 values from the permuted data were compared with the R^2 values from the above actual data (using the Wilcoxon rank sum test).

The overfitting problem

K-fold cross validation was used to estimate whether the above procedure had an overfitting problem. In our analysis, the K value was 11 (each fold had 9 patients). For each attribute, we examined whether the objective function, which was established with data from 90 patients, could predict the performance of the remaining 9 patient when his or her imaging data were introduced into the function. Specifically, we first conducted the NSLM analysis as described above except that the behavioral and imaging data of 99 patients were replaced with those of 90 patients. The objective function with the maximum R^2 value was selected as the testing function. Then, we input the imaging data from the remaining 9 patient into the testing function and obtained the predicted score of the patient. Thus, we obtained a predicted behavioral score for each patient. Finally, we computed the correlation values between the actual and predicted values in the specific node value (the node number for the z score attribute subnetwork) of the optimal subnetwork for each attribute across the 99 patients. The root mean squared error (RMSE) is an indicator that can measure the model performance, for the value from 0 to $+\infty$. We calculated

RMSE using the following formula (Chai and Draxler 2014):

$$\mathrm{RMSE} = \sqrt{\frac{1}{n}\sum_{i=1}^{n} e_i^2},$$

where n is the samples of the model, and e is the errors. A lower RMSE score indicates better model performance (Chai and Draxler 2014). We run the 11-fold cross-validation three times to get the highest R value and the average RMSE value.

The method problem

We compared the NLSM with the univariate and multivariate white matter analysis, to check whether the NLSM was more robust than the previous analysis methods. In univariate analysis, we conducted tract-based correlations (van Kooij et al. 2012) between each tract and behavioral performance to identify the highest correlated tracts. In multivariate analysis, we ran the nonnegative matrix factor (NMF) analysis (Lange et al. 2004; Sotiras et al. 2015, 2017; Bouchard et al. 2022). Specifically, the NMF method was used for dimension reduction in the matrix X of 998 tracts × 99 patients. For each component value, the matrix could be divided into two submatrices, denoted as W and H. Reconstruction error was measured by the difference between X and $W \times H$ (Bouchard et al. 2022). To measure the reproducibility, the data were divided into two split samples with similar demographic information and ran the NMF instructions at the same component value (we randomly deleted one person so that the matrix could be split in half and repeated a hundred times). Then, a Hungarian algorithm (Kuhn 1955) was used to match the two samples and the inner-product (range from 0 to 1) was also used to calculate the overlap between the two split samples (Bouchard et al. 2022). The reproducibility value for each component was determined as the median inner-product value.

Subnetwork analysis for subgroups

As mentioned in the neurocomputational model, the whole patient group exhibited diverse hemispheric-injury patterns, which might have different contributions to our results due to the recovery mechanism (Chang and Lambon Ralph 2020). To account for the lateralization pattern in different hemispheric-injury subgroups, we divided the whole patient group into three subgroups (left-lesion, bi-lesion, and right-lesion subgroups). Then, we utilized their z scores to run the NLSM method and calculate the LI values. To determine whether the lateral modulation effect was specific to different lesion hemispheres, we also measured the effect concerning different etiology. Regarding lesion etiology, we also divided the whole patient group into three subgroups (infarction, hemorrhage, and trauma subgroups). Then, we used their z scores to run the NLSM method and calculate the LI values. In this analysis, we calculated subnetworks for all language and nonlanguage attributes, but we more focused on the language subnetworks.

Results

Behavioral performance

The response accuracies in language and nonlanguage tasks for each of six attributes were illustrated in Fig. 1. Compared with the healthy controls, the patients' ability to process each attribute was impaired in both the language task (healthy controls: 93% ± 7% vs. patients: 84% ± 13%; $t = 11.243$, $P < 0.001$) and nonlanguage task (83% ± 13% vs. 72% ± 19%; $t = 9.636$, $P < 0.001$). All the attributes except for manipulation showed larger impairments in the nonlanguage task than the language task: form (language task: 86% ± 12% vs. nonlanguage task: 75% ± 12%; $t = 7.92$, $P < 0.001$), color (84% ± 14% vs. 63% ± 17%; $t = 14.71$, $P < 0.001$), motion (84% ± 11% vs. 52% ± 18%; $t = 17.49$, $P < 0.001$), sound (78% ± 11% vs. 73% ± 14%; $t = 4.19$, $P < 0.001$), and function (92% ± 9% vs. 89% ± 13%; $t = 2.43$, $P < 0.05$). The manipulation attribute reflected similar levels impairment between the two tasks (81% ± 15% vs. 80% ± 15%; $t = 0.89$, $P > 0.10$). The Supplementary Table 2 encompassed the mean values, SDs, and ranges of the participants' raw data.

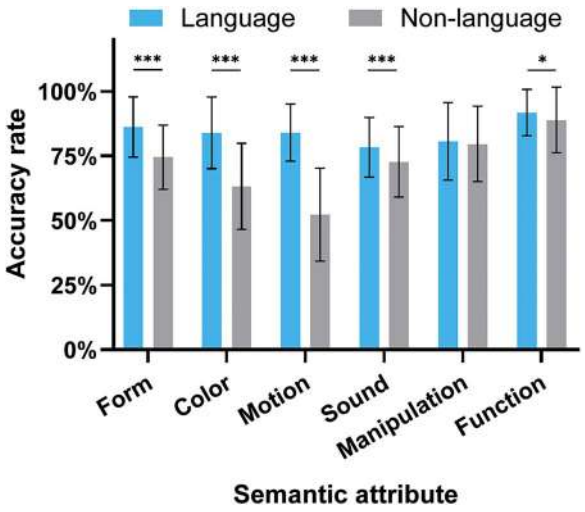

Fig. 1. Raw accuracy rate of each attribute in language and nonlanguage tasks. Error bars indicate the SD. *$P < 0.05$; ***$P < 0.001$.

For raw scores, we calculated the correlation between the 12 attribute tasks (see Supplementary Fig. 1). We found that the correlation between each pair of tasks was significant (FDR corrected, qs < 0.05). Moreover, the correlations between the language tasks (range: 0.59–0.83) were especially significant (FDR corrected, qs < 0.001).

Whole-brain white matter connection of patients

The lesions of the patients were widely distributed in the whole brain, and most patients had lesions in the insula and its surrounding neural tissues (Fig. 2a). In the whole brain network of 90 AAL nodes, there were 998 tracts in 842 healthy participants (Yeh et al. 2018; Griffis et al. 2020). Across the 99 patients, all but four tracts ($n = 994$) had lesions (Fig. 2b). The damaged tracts included 303 left intratracts, 250 right intratracts, and 441 intertracts that connected regions in the left hemisphere, the right hemisphere, and both hemispheres, respectively. The number of intertracts was statistically equivalent with that of left intratracts ($\chi^2 = 2.90$, $P = 0.09$) and right intratracts ($\chi^2 = 3.51$, $P = 0.06$). However, the numbers of left and right intratracts were comparable ($\chi^2 = 0.04$, $P = 0.85$). Most tracts (99.6% of these tracts) were lesioned in at least one patient (99.3% of left intratracts; 99.2% of right intratracts; and 100% of intertracts).

Subnetworks underlying each attribute processing and their laterization

The R value of all our optimal subnetwork results was overviewed in Table 2. In Table 2, only two subnetworks were uncorrected, two subnetworks were *FDR* corrected $q < 0.10$, and other subnetworks were all *FDR* corrected $q < 0.05$, which means our results were

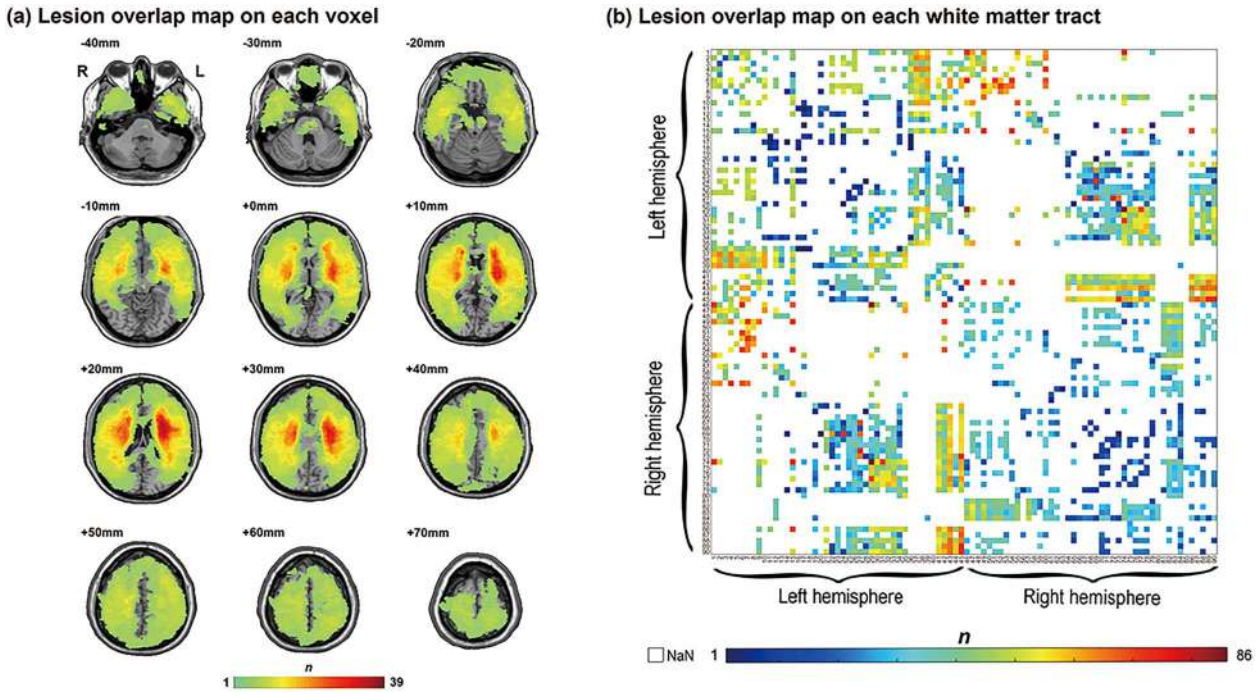

Fig. 2. Lesion overlap maps for each voxel and each white matter tract across 99 patients. The *n* value of each voxel in Fig. 2a or each tract in Fig. 2b denotes the number of patients with lesions in that voxel or tract. The tracts in Fig. 2b connect the 90 AAL regions. Details about the regions are provided in Supplementary Table 3.

reliable. The LI values (node LI, edge LI, and network LI) of all our optimal subnetwork results were overviewed in Supplementary Table 4. In language subnetworks, most subnetworks showed the left-lateral pattern except for the left-lesion subgroup.

Applying the NLSM method (Li, Song, et al. 2021), we identified 12 subnetworks supporting the 6 attributes with respect to language and nonlanguage tasks. Three LI values were calculated for each subnetwork corresponding to its node number, edge number, and the sum of the nodal degrees (Figs. 3 and 4).

Overall, for most attributes, the subnetworks corresponding to the language task than nonlanguage task contained more nodes (form: 11 vs. 8; color: 10 vs. 6; motion: 8 vs. 8; sound: 13 vs. 7; manipulation: 10 vs. 10; function: 6 vs. 6) and more edges (form: 20 vs. 8; color: 11 vs. 7; motion: 11 vs. 7; sound: 17 vs. 5; manipulation: 11 vs. 7; function: 6 vs. 6). This finding demonstrates that the subnetworks for the language task than those in nonlanguage task had more complicated anatomical structure.

The LI values of subnetworks in the language task were consistently higher than 0.20 (node LI: 0.33–1; edge LI: 0.67–1; nodal degree LI: 0.67–1) (see Fig. 3 and Supplementary Table 4). This suggests that language processing of each of the six attributes was supported by a left-lateralized subnetwork. In the nonlanguage task (see Fig. 4 and Supplementary Table 4), LI values of subnetworks for three of attributes (color, manipulation, function) were higher than 0.20 (node LI: 0.60–1; edge LI: 0.71–1; nodal degree LI: 0.71–1), indicating strongly left lateralization of these subnetworks. Those of the form attribute were lower than −0.20 (node LI: −0.25; edge LI: −0.38; nodal degree LI: −0.43), indicating the right lateralization of these subnetworks. Those of the motion and sound attributes ranged from −0.20 to 0.20 (node LI: 0–0.14; edge LI: 0–0.20; nodal degree LI: 0–0.20), indicating the bilateralization of these subnetworks. We conducted an additional group analysis consisting all right-handed individuals (excluding 6 patients) to assess the potential influence of handedness on the lateralization pattern. These results (see Supplementary Figs 2 and 3; Table 2 and Supplementary Table 4) demonstrated that the language and nonlanguage lateralization patterns were consistent with the subnetworks in 99-patient group. Furthermore, subnetworks removed patients who were not impaired in each attribute task was measured, and showed the highly similar lateralization patterns (see Supplementary Figs 4 and 5). The two additional analyses declared that the handedness and ceiling effect might had no influence on the lateralization patterns.

Validation analysis results

The task difference problem

The NLSM analysis using the corrected-*t* scores instead of the normalized behavioral accuracy obtained an additional 12 subnetworks and their LIs were calculated (see Figs. 5 and 6 and Supplementary Table 4). These new subnetworks and their *R* values were highly similar to those obtained from normalized accuracy data (see Table 2 and Figs. 3 and 4). Specifically, for language and nonlanguage attributes, the overall numbers of nodes and edges between *z* score and *t* score subnetworks were similar, and the overlap rate of the nodes between them was high (see Table 3). More importantly, the lateralization of each attribute subnetwork except for the nonlanguage form attribute subnetwork was consistent between old and new subnetworks (see Supplementary Table 4). The LI values of each *t* score subnetwork in the language task were consistently higher than 0.20 (node LI: 0.56–1; edge LI: 0.88–1; nodal degree LI: 0.88–1). This suggests that language processing of each of the six attributes was supported by a left-lateralized subnetwork. In the nonlanguage task of *t* score, the LI values of three attributes (color, manipulation, function) were higher than 0.20 (node LI: 0.56–1; edge LI: 0.67–1; nodal degree LI: 0.67–1), indicating left lateralization of these subnetworks. Those of form, motion, and sound attributes (except

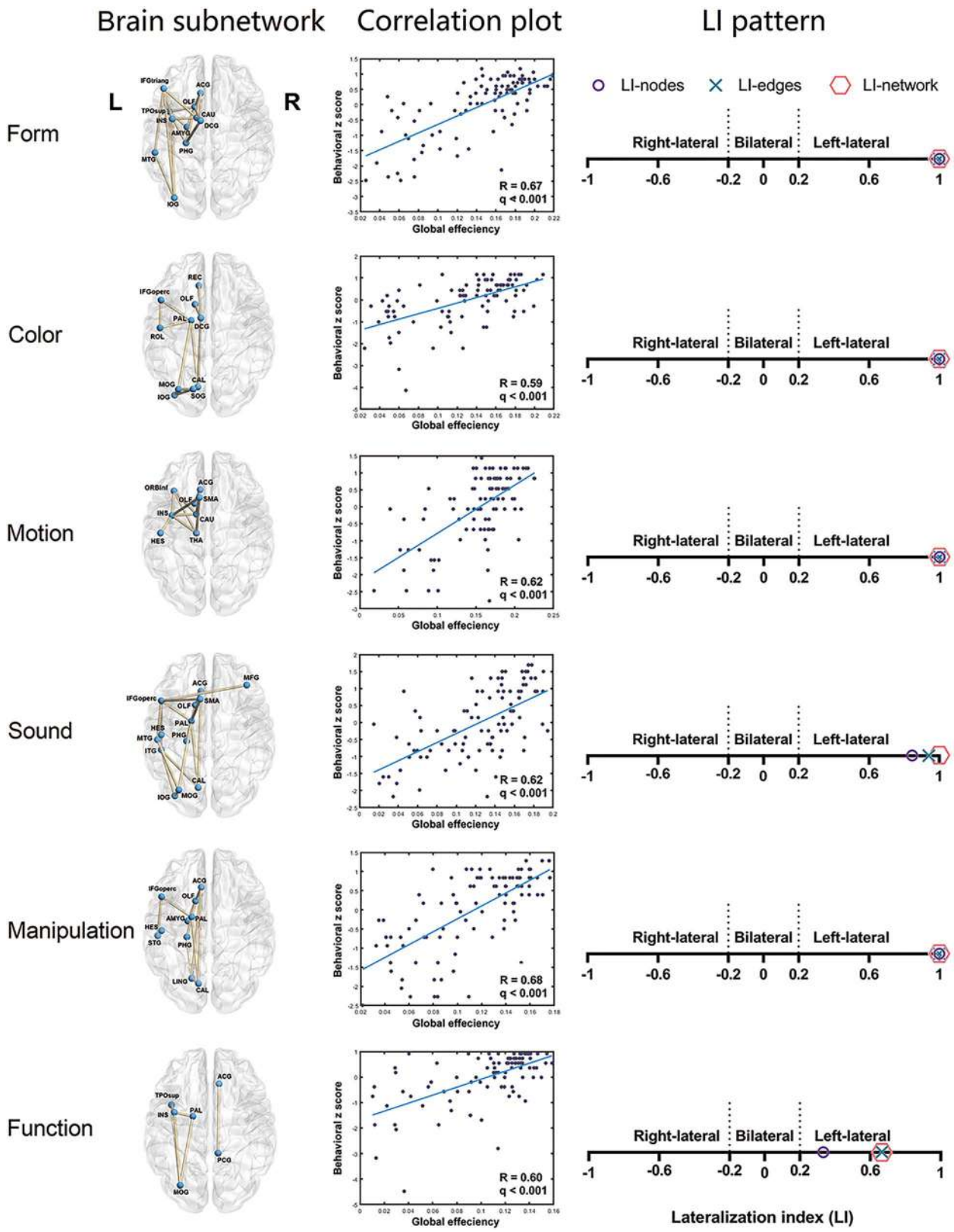

Fig. 3. The optimal subnetwork for the whole patient group ($n = 99$) underlying the processing of each language attribute processing and its LI. The correlation plot illustrates a relationship between the global efficiency of patients' networks and their performance. ACG = anterior cingulate and paracingulate gyrus; AMYG = amygdala; CAL = calcarine fissure and surrounding cortex; CAU = caudate nucleus; DCG = median cingulate and paracingulate gyrus; HES = heschl gyrus; IFGoperc = inferior frontal gyrus, opercular part; IFGtriang = inferior frontal gyrus, triangular part; INS = insula; IOG = inferior occipital gyrus; ITG = inferior temporal gyrus; LING = lingual gyrus; MFG = middle frontal gyrus; MOG = middle occipital gyrus; MTG = middle temporal gyrus; OLF = olfactory cortex; ORBinf = inferior frontal gyrus, orbital part; PAL = lenticular nucleus, pallidum; PCG = posterior cingulate gyrus; PHG = parahippocampal gyrus; REC = gyrus rectus; ROL = rolandic operculum; SMA = supplementary motor area; SOG = superior occipital gyrus; STG = superior temporal gyrus; THA = thalamus; TPOsup = temporal lobe: superior temporal gyrus.

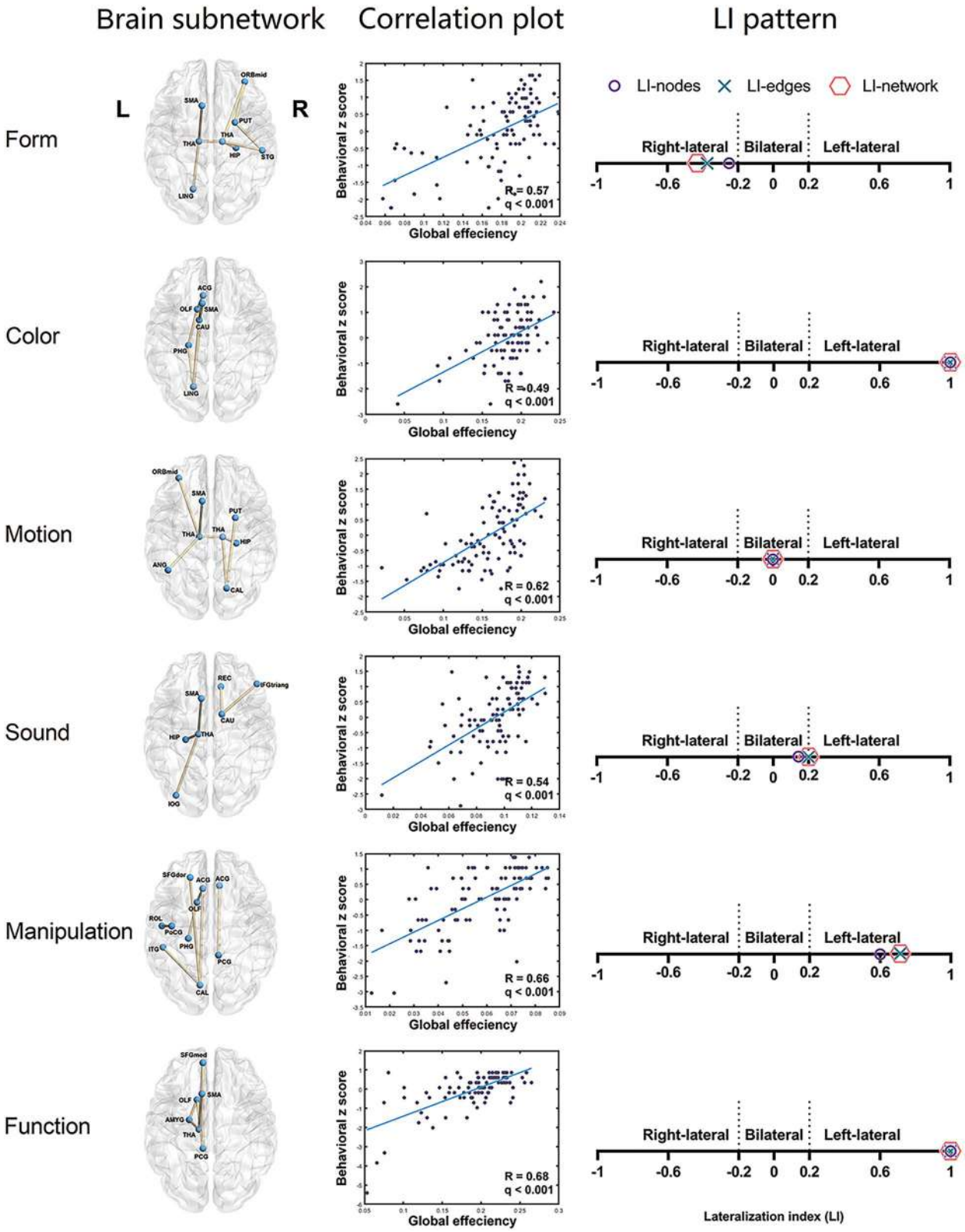

Fig. 4. The optimal subnetwork for the whole patient group ($n = 99$) underlying the processing of each nonlanguage attribute processing and its LI. The correlation plot illustrates a relationship between the global efficiency of patients' networks and their performance. ANG = angular gyrus; HIP = hippocampus; ORBmid = middle frontal gyrus, orbital part; PoCG = postcentral gyrus; PUT = lenticular nucleus, putamen; SFGdor = superior frontal gyrus, dorsolateral; SFGmed = superior frontal gyrus, medial. The complete names of the other abbreviations are provided in previous figure.

Table 2. FDR-corrected significance of *R* values for the optimal subnetworks across various patient subgroups.

Attribute		Whole patient group using *z* scores (*n* = 99)	Whole patient group using *t* scores (*n* = 99)	Right-handed subgroup (*n* = 93)	Trauma subgroup (*n* = 17)	Infarction subgroup (*n* = 46)	Hemorrhage subgroup (*n* = 30)	Left-lesion subgroup (*n* = 37)	Right-lesion subgroup (*n* = 23)	Bi-lesion subgroup (*n* = 39)
Language	Form	0.67***	0.69***	0.68***	0.93***	0.71***	0.89***	0.66***	0.69**	0.83***
	Color	0.59***	0.62***	0.61***	0.93***	0.74***	0.84***	0.57*	0.61*	0.79***
	Motion	0.62***	0.63***	0.65***	0.91***	0.75***	0.73***	0.75***	0.60*	0.63**
	Sound	0.62***	0.64***	0.65***	0.86***	0.73***	0.72**	0.73***	0.59*	0.75***
	Manipulation	0.68***	0.68***	0.68***	0.94***	0.75***	0.88***	0.68***	0.67**	0.85***
	Function	0.60***	0.63***	0.62***	0.84**	0.68***	0.80***	0.61**	0.55#	0.77***
Nonlanguage	Form	0.57***	0.55***	0.56***	0.84**	0.70***	0.78***	0.66***	0.68**	0.77***
	Color	0.49***	0.48***	0.50***	0.87**	0.57**	0.75***	0.63**	0.57*	0.71***
	Motion	0.62***	0.59***	0.61***	0.91***	0.66***	0.74***	0.53*	0.74**	0.79***
	Sound	0.54***	0.49***	0.53***	0.92***	0.67***	0.56#	0.42	0.70**	0.85***
	Manipulation	0.66***	0.64***	0.68***	0.72*	0.67***	0.84***	0.67**	0.49	0.80***
	Function	0.68***	0.68***	0.70***	0.91***	0.73***	0.88***	0.76***	0.80***	0.86***

Note. #false discovery rate (FDR)-corrected $q < 0.10$; *$q < 0.05$; **$q < 0.01$; ***$q < 0.001$.

Table 3. The comparison between results of *z* and *t* scores.

		The number of nodes			The number of edges		
		z score	*t* score	Common nodes	*z* score	*t* score	Common edges
Language	Form	11	11	9	20	17	14
	Color	10	11	10	11	12	11
	Motion	8	11	5	11	15	4
	Sound	13	13	8	17	16	6
	Manipulation	10	10	9	11	12	9
	Function	6	9	6	6	16	6
Nonlanguage	Form	8	7	5	8	8	4
	Color	6	6	6	7	7	7
	Motion	8	8	4	7	12	3
	Sound	7	8	6	5	5	4
	Manipulation	10	9	8	7	6	5
	Function	6	6	6	6	6	6

for the node LI of sound attribute was 0.25) ranged from −0.20 to 0.20 (node LI: −0.14–0; edge LI: −0.13–0.20; nodal degree LI: −0.14–0.20), indicating the bilateralization of these subnetworks. These results demonstrate that the asymmetric differences among the 12 attribute-relevant subnetworks might arise from the differences in representations of cognition rather than tasks.

The random chance problem

We repeated the NLSM analysis as above, except that each patient's behavioral score was randomly matched with the brain imaging data of a different patient. Thus, we obtained a new set of R^2 values from the permuted subnetworks for each attribute. For all the language attributes, these permuted R^2 values were found to be significantly lower than those of the actual subnetworks using the Wilcoxon rank sum test (form: 0.08 ± 0.05 vs. 0.44 ± 0.01, $Z = 63.24$, $P < 0.001$; color: 0.08 ± 0.05 vs. 0.33 ± 0.02, $Z = 63.21$, $P < 0.001$; motion: 0.08 ± 0.05 vs. 0.38 ± 0.01, $Z = 63.25$, $P < 0.001$; sound: 0.37 ± 0.01 vs. 0.37 ± 0.01, $Z = 63.24$, $P < 0.001$; manipulation: 0.0785 ± 0.05 vs. 0.44 ± 0.02, $Z = 63.24$, $P < 0.001$; function: 0.08 ± 0.05 vs. 0.36 ± 0.01, $Z = 63.27$, $P < 0.001$; see Fig. 5). For all the nonlanguage attributes, these permuted R^2 values were also found to be significantly lower than those of the actual subnetworks (form: 0.08 ± 0.05 vs. 0.31 ± 0.01, $Z = 63.21$, $P < 0.001$; color: 0.08 ± 0.04 vs. 0.23 ± 0.01, $Z = 62.67$, $P < 0.001$; motion: 0.07 ± 0.04 vs. 0.37 ± 0.01, $Z = 63.24$, $P < 0.001$; sound: 0.08 ± 0.04 vs. 0.26 ± 0.03, $Z = 63.03$, $P < 0.001$; manipulation: 0.07 ± 0.05 vs. 0.41 ± 0.02, $Z = 63.24$, $P < 0.001$; function: 0.09 ± 0.06 vs. 0.44 ± 0.02, $Z = 63.14$, $P < 0.001$; see Fig. 6). These findings demonstrated that these attribute subnetworks were not obtained through random chance.

The overfitting problem

We used data from 90 patients to build the model, and the remaining 9 patient's data were used to conduct a test at the specific node value in attribute task. For each patient, we obtained a predicted behavioral score for each attribute task for the specific node value of the optimal network. For the attributes in the language task, the predicted scores were significantly correlated with the actual scores across the 99 patients for the specific node value of the optimal subnetwork (form: $n = 11$, $R = 0.51$,

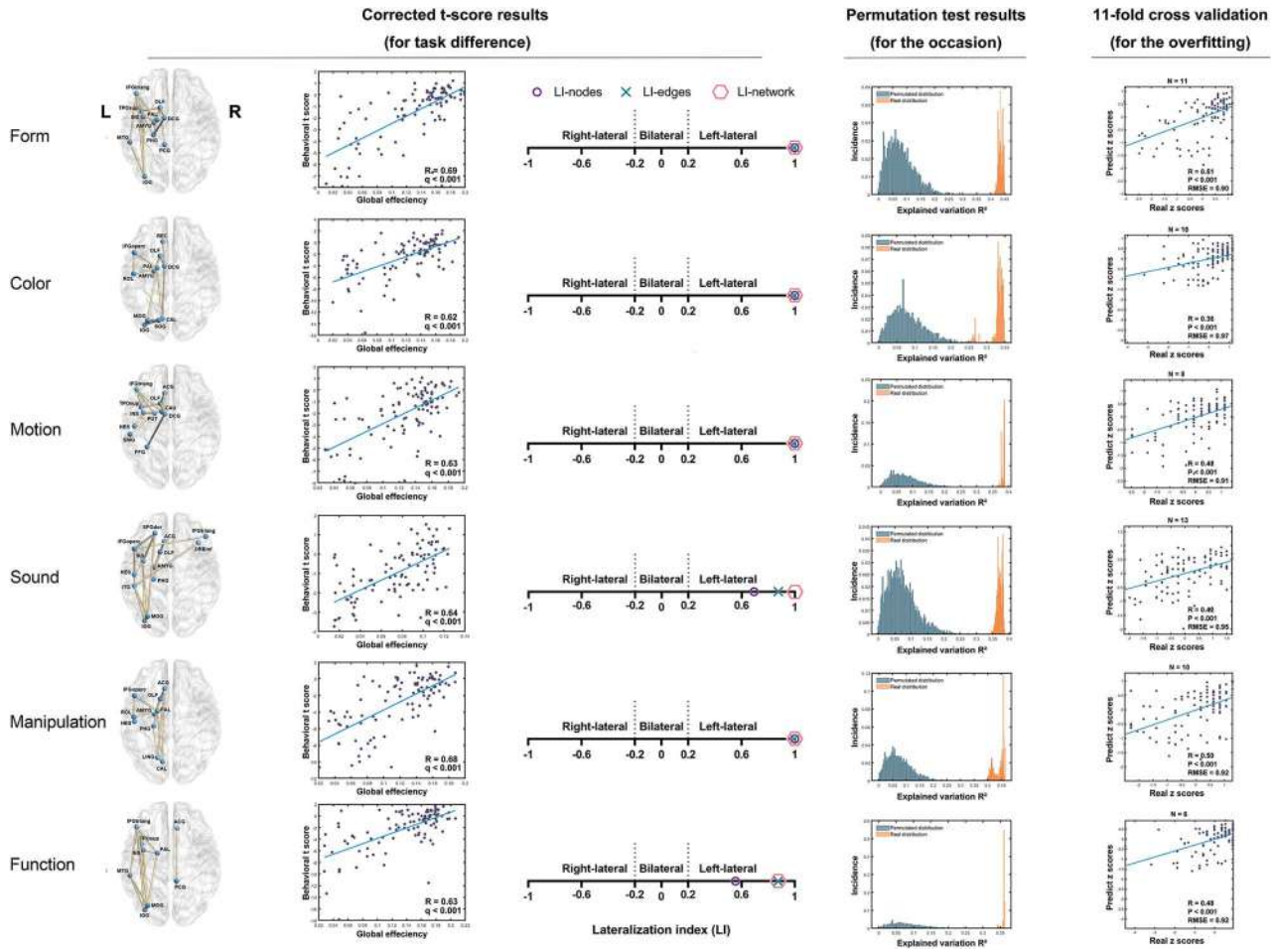

Fig. 5. Results of the validation analyses of language attribute networks. The left three columns show the correct *t* score results underlying language attribute processing and their LIs. The right two columns show the permutation and 11-fold results of the validation analyses for subnetworks underlying language attribute processing. The correlation plot demonstrates that the global efficiency of patients' networks can significantly correlate with their performance**.** The *N* value in the final column is the optimal node value in *z* score results. FFG = fusiform gyrus; SMG = supramarginal gyrus. The complete names of the other abbreviations are provided in previous figures.

$P < 0.001$, average RMSE = 0.90; color: $n = 10$, $R = 0.36$, $P < 0.001$, average RMSE = 0.97; motion: $n = 8$, $R = 0.48$, $P < 0.001$, average RMSE = 0.91; sound: $n = 13$, $R = 0.42$, $P < 0.001$, average RMSE = 0.95; manipulation: $n = 10$, $R = 0.50$, $P < 0.001$, average RMSE = 0.92; function: $n = 6$, $R = 0.48$, $P < 0.001$, average RMSE = 0.92; see Fig. 5). For nonlanguage attributes, the predicted scores were also significantly correlated with the actual scores across the 99 patients for the specific node value of the optimal subnetwork (form: $n = 8$, $R = 0.36$, $P < 0.001$, average RMSE = 0.97; color: $n = 6$, $R = 0.26$, $P < 0.05$, average RMSE = 1.01; motion: $n = 8$, $R = 0.47$, $P < 0.001$, average RMSE = 0.94; sound: $n = 7$, $R = 0.36$, $P < 0.001$, average RMSE = 0.96; manipulation: $n = 10$, $R = 0.45$, $P < 0.001$, average RMSE = 0.95; function: $n = 6$, $R = 0.44$, $P < 0.001$, average RMSE = 1.00; see Fig. 6). These results suggest that the NLSM procedures used to obtain the attribute subnetworks should not have an overfitting problem.

The method problem

For univariate analysis, the 10 most significant tracts associated with each attribute were selected as representative tracts for that attribute, the highest *R* value, and the LI value was in Supplementary Table 5. In language tasks, the LI consistently indicated a left-lateral pattern. However, in nonlanguage tasks, the LI exhibited diverse patterns: left-lateral for color, manipulation, and function; bilateral for sound; and right-lateral for form and motion tasks. For multivariate analysis, we finally selected 7 components based on their peak reproducibility and proximity to the lowest reconstruction error (Bouchard et al. 2022). Each tract had a weighted value in each component. We then calculated the LI values in each component by the tract weight and measure the correlation between patients' behavioral *z* scores and the tract component weight in patients to find the highest correlation component for each task (see Supplementary Table 5). We found in language tasks that the six tasks were all left-lateral (LI = 1). For nonlanguage tasks, four tasks were left-lateral (color, sound, manipulation, and function attributes) and two tasks were right-lateral (form and motion attributes). These lateralization patterns for univariate and multivariate analysis were similar to that of NLSM. The two-way ANOVA analysis (factoring in language and nonlanguage task type × univariate, multivariate, and NLSM method) revealed significant main effects in both task types ($F = 9.334$, $P < 0.05$) and methods ($F = 25.679$, $P < 0.001$), with no observed interaction. One-way ANOVA analysis indicated significant method main effects in all tasks ($F = 20.937$, $P < 0.001$). Post hoc tests (see Supplementary Fig. 6) indicated that in both language and all tasks, the *R* value of NLSM was significantly higher than that of the univariate and multivariate methods.

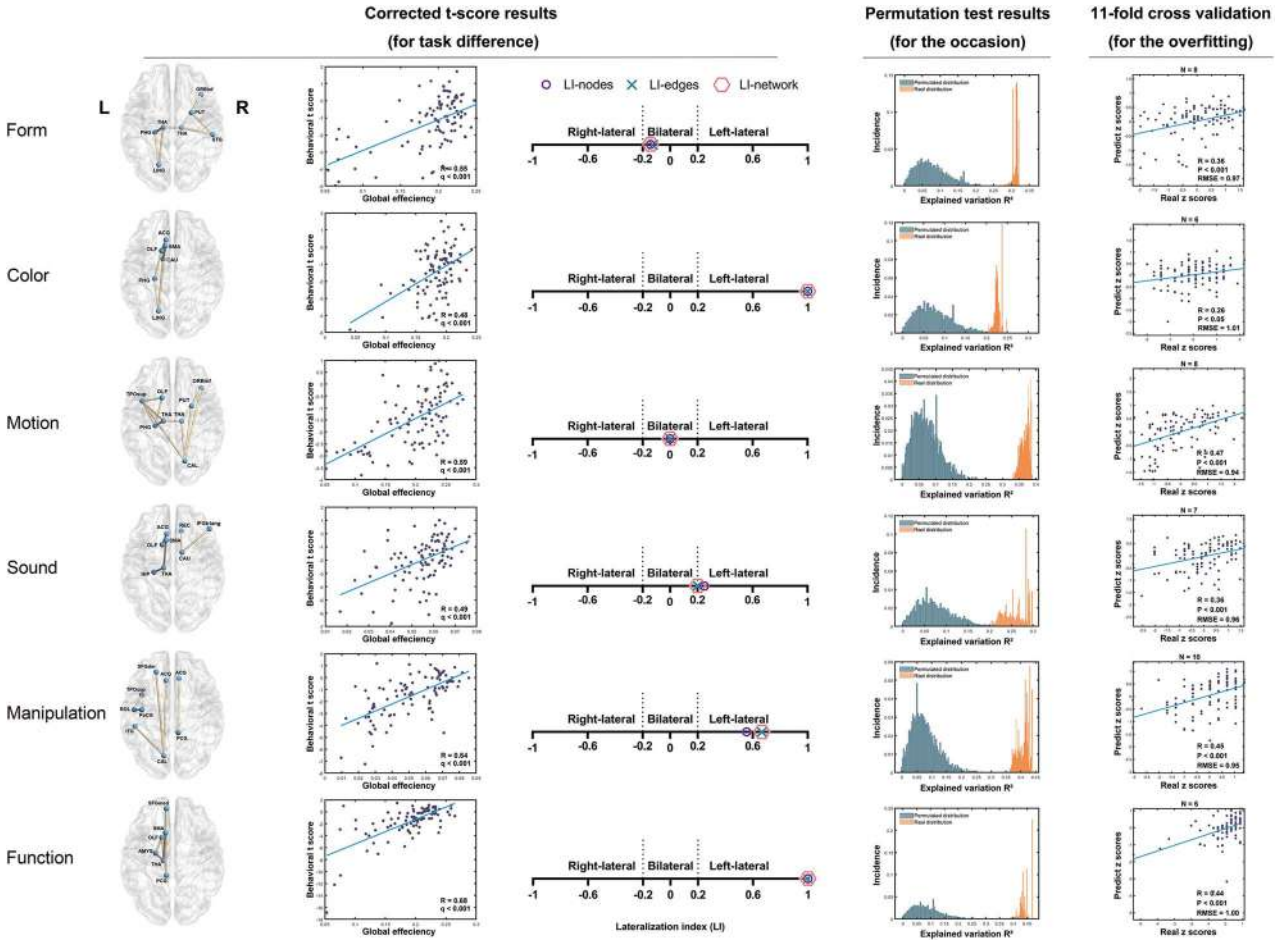

Fig. 6. Results of the validation analyses of nonlanguage attribute networks. The left three columns show the correct *t* score results underlying nonlanguage attribute processing and their LIs. The right two columns show the permutation and 11-fold results of the validation analyses for subnetworks underlying nonlanguage attribute processing. The correlation plot demonstrates that the global efficiency of patients' networks can significantly correlate with their performance**.** The *N* value in the final column is the optimal node value in z score results. The complete names of the abbreviations are provided in previous figures.

For nonlanguage tasks, the NLSM was significantly higher than the multivariate method. These findings demonstrate that the NLSM holds distinct advantages in identifying behaviorally relevant subnetworks when compared with traditional univariate and multivariate white matter tracts analyses.

Subnetwork analysis for subgroups

We observed that among the patients, 37 exhibited lesions only in the left hemisphere (whose lesion tracts in right hemisphere was less than 2, and referred to as the left-lesion subgroup), 23 patients displayed lesions solely in the right hemisphere (whose lesion tracts in left hemisphere was less than 2, and referred to as the right-lesion subgroup), and 39 patients demonstrated lesions in both hemispheres (referred to as the bi-lesion subgroup). The three subgroups did not have a statistical significance ($\chi^2 = 4.61$, $P = 0.10$). The lesioned intertracts number in bi-lesion subgroup was indeed the highest in three subgroups and was significantly higher than the left subgroup (see Supplementary Table 6).

For the language subnetworks of patient lesion subgroups (see Fig. 7 and Supplementary Table 4), patients with bilateral lesions exhibited left-lateralized subnetworks across all six attributes (node LI: 0.78–1; edge LI: 0.79–1; nodal degree LI: 1). Patients with left hemisphere lesions demonstrated bilateral or right-lateralized subnetworks except for the color attribute (node LI: −0.45–0; edge LI: −0.50–−0.09; nodal degree LI: −0.60–−0.14; LIs in color attribute: 0.33), while patients with right hemisphere lesions displayed bilateral or left-lateralized subnetworks except for the sound attribute (node LI: 0–1; edge LI: 0–1; nodal degree LI: 0–1; LIs in color attribute: −1). These results indicated that lesion in different hemispheres would influence the lateralization pattern in patients and strongly supported the predictions of this neurocomputational model (Chang and Lambon Ralph 2020). In nonlanguage subnetworks, the lateralization patterns also tended to transfer into the hemisphere which was undamaged (see Supplementary Table 4).

Furthermore, we observed that among the patients, 30 patients suffered lesions from hemorrhage (referred to as the "hemorrhage subgroup"), 46 patients suffered lesions from infarction (referred to as the "infarction subgroup"), and 17 suffered lesions from trauma (referred to as the "trauma subgroup"). For different etiology in language subnetworks (see Supplementary Fig. 7), we found left-lateral results in all the language tasks across the three subgroups (see Supplementary Table 4) except for node LI for form language attribute in trauma subgroup (node LI: 0.33–1; edge LI: 0.25–1; nodal degree LI: 0.33–1; node LI in trauma subgroup: 0.19). These results were consistent with the language subnetworks for 99 patient group, which indicated that different etiology could not affect the lateralizaition pattern in language

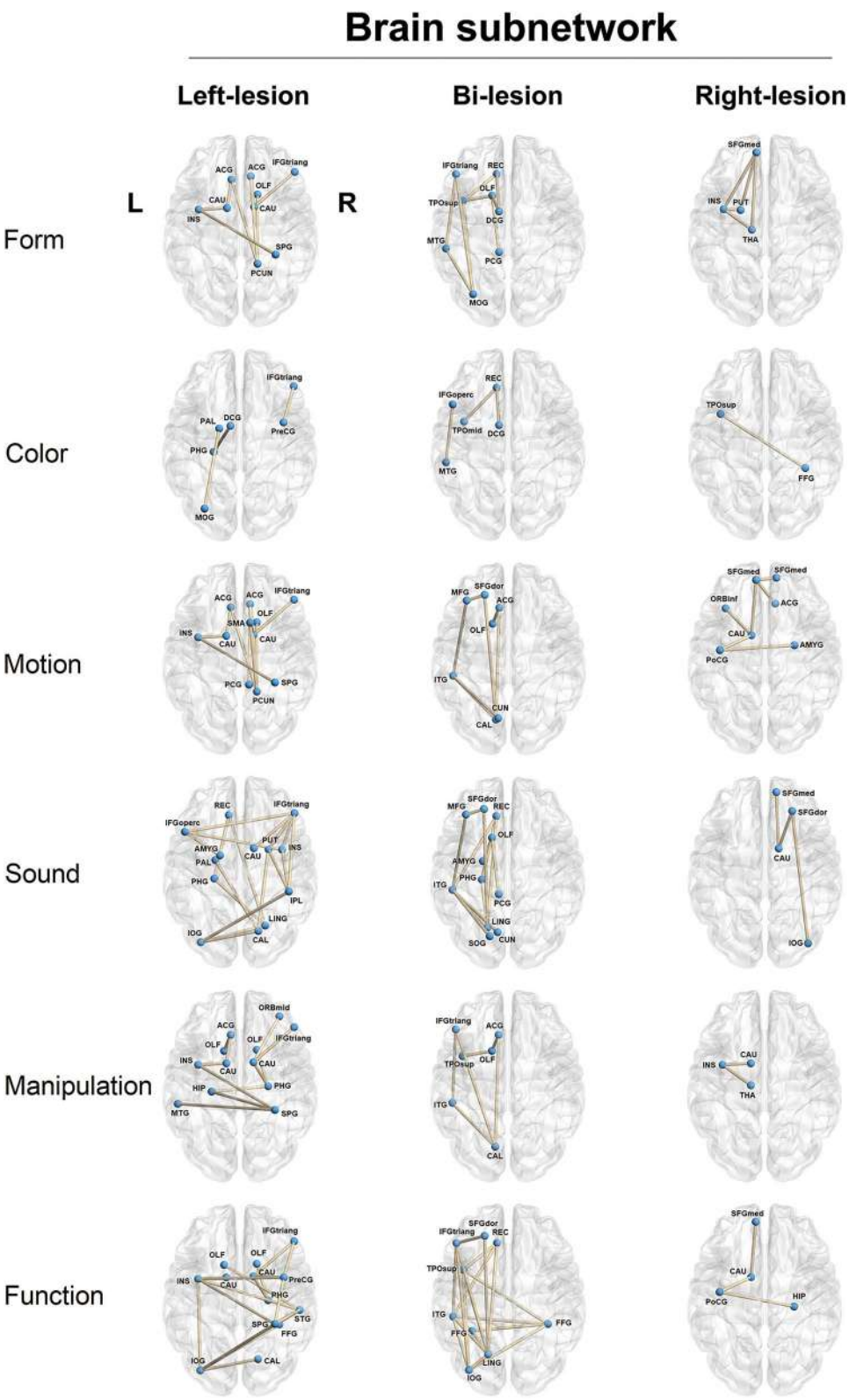

Fig. 7. Language optimal subnetworks for different lesion subgroups. CUN = cuneus; IPL = inferior parietal but not supramarginal and angular gyrus; PCUN = precuneus; PreCG = precentral gyrus; SPG = superior parietal gyrus; TPOmid = temporal lobe: middle temporal gyrus. The complete names of the other abbreviations are provided in previous figures. The correlation *R* value was in Table 2 and the LI values were in Supplementary Table 4.

processing. In nonlanguage subnetworks, the lateralization patterns were also similar to the whole group, while the nonlanguage subnetworks of trauma subgroup were more left-lateral (see Supplementary Table 4).

Discussion

Employing the NLSM method in 99 patients with brain injuries, we explored the lateralization pattern of the white matter subnetwork supporting six attributes (form, color, motion,

sound, manipulation, and function) in language processes for the whole group and different subgroups to investigate the neurocomputational model (Chang and Lambon Ralph 2020). Our findings revealed a consistent left-lateral pattern across all subnetworks involved in language processing within the whole patient group. In contrast, nonlanguage processing exhibited different lateralization patterns: the subnetwork of form attribute was right-lateralized, those of motion and sound attributes were bilateral, and those of color, manipulation, and function attributes were left-lateralized. Validation analysis confirmed that these results had no task difference, random chance, overfitting, or method problems. Regarding the language subnetworks in different lesion subgroups, the results showed that lesions in one hemisphere could be compensated by another hemisphere, while the bi-lesion subgroup showed the left hemisphere language dominance. In different etiology subgroups, the lateralization pattern was consistent with that in the whole 99 patient group. These results suggested that the patterns of lesion subgroups were specific to hemispheres and matched the neurocomputational model (Chang and Lambon Ralph 2020).

Lateralization pattern for language and nonlanguage processing

We observed that language function in the patient group exhibited a strong left-lateralization pattern across many attributes, which aligns with previous researches and the neurocomputational model (Chang and Lambon Ralph 2020). Since Broca (1861) discovered that damage to the left hemisphere resulted in language deficits, the lateralization of language function has been broadly investigated. Some studies have supported that language processing was left-lateralized and nonlanguage processing was right-lateralized or bilateral (Thierry et al. 2003; Thierry and Price 2006; Dick et al. 2007; Butler et al. 2009; Gainotti 2015). However, other studies have highlighted the importance of the right hemisphere in language function (Lindell 2006; Hartwigsen and Siebner 2012). A series of recent studies also discovered that specific attributes could modulate language processing in both hemispheres in healthy individuals (Fernandino, Binder, et al. 2016; Fernandino, Humphries, et al. 2016; Popp et al. 2019; Kuhnke et al. 2020). In our study of brain-damaged patients, we found that, across these attributes, the language subnetworks consistently exhibited a left-lateralized pattern.

We did not find a distinct bilateral or right-lateral effect for any attribute in language processing, suggesting that language processing relied more on the left hemisphere than the right hemisphere in brain-damaged individuals. However, it is important to note that language processing is not entirely left-lateralized in healthy and even in patient individuals, and the right hemisphere might play a role (Lambon Ralph et al. 2017). In our study, the form, color, and manipulation attributes displayed clearly left-lateralized networks, but in other attributes (motion, sound, and function), some right nodes were involved in patients. This suggested that the right hemisphere contributed to the language processing of these attributes in brain-damaged individuals. Early studies, which focused on language processing, highlighted the role of left regions, such as the left anterior temporal lobe (ATL), in storing different types of language information, independent of the input (e.g. words or sounds), output (e.g. speaking or drawing), or the type of language context (e.g. living things, man-made objects, and abstract ideas) (Patterson et al. 2007; Gainotti 2015). Recent research suggested that the right ATL might also be involved in language processing although the dominance of the left hemisphere was maintained (Lambon Ralph et al. 2017).

Unlike language processing, nonlanguage functions have previously shown bilateral or right-lateralized patterns (Thierry and Price 2006; Gainotti 2015; Sun et al. 2017). Three different lateralization patterns were demonstrated in our results: the network for the form attribute was right-lateralized, the networks for motion and sound attributes were bilateral, and the networks for color, manipulation, and function attributes were left-lateralized. Previous research discovered that both hemispheres were activated in subnetworks representing the nonlanguage processing of form, color, motion, and sound (Miceli et al. 2001; Thierry and Price 2006; Vinberg and Grill-Spector 2008; Stasenko et al. 2014). These lateralization patterns are mostly consistent with existing literature and enhance the reliability of our language subnetwork results. Regarding the form attribute, previous studies indicated that patients with bilateral brain damage experienced visual form agnosia, leading to an inability to recognize object forms (Karnath et al. 2009; Bridge et al. 2013). However, our study found right-lateralized white matter network involved in nonlanguage processing form attribute. This difference may be because the visual form agnosia, typically resulting from carbon monoxide poisoning, often leads to a widespread loss of neurons diffusely across the whole brain (Karnath et al. 2009). In this case, the asymmetry of the form attribute network needs to be further elucidated. For the color attribute, a study found that patients with color agnosia struggled to match objects with their typical colors and had lesions in the left ventral cortical visual stream (Siuda-Krzywicka and Bartolomeo 2020). Another study found that color might be a more abstract attribute and is related to language processing because it requires individuals to ignore differences between objects, such as their form and function (Siuda-Krzywicka et al. 2020). For the manipulation and function attributes, both healthy and brain-damaged individuals exhibit a left-dominant pattern (Buxbaum and Saffran 2002; Boronat et al. 2005; Lesourd et al. 2021). This could be attributed to the left-lateralized processing of tool use (Peeters et al. 2009; Vingerhoets et al. 2011), where using a tool necessitates forming and translating an internal representation of the required information to perform associated actions (Lesourd et al. 2021).

To avoid the potential influence of differences between language and nonlanguage brain areas on our results, we compared nonoverlapping language and nonlanguage regions within our findings and showed no significance (see Supplementary Table 7). Furthermore, we conducted a comparative analysis using the results of a prior meta-analysis (Binder et al. 2009). Specifically, we evaluated the contrast between left language and nonlanguage brain regions and assessed the damage to left language brain regions compared to right homotopic brain regions in meta-analysis results (see Supplementary Table 8). Meta-analysis results suggested that the extent of damage to language and nonlanguage brain regions was similar and had no significance. For homotopic region pairs in both hemispheres of the meta-analysis, the left brain region might be lesion more than the right.

Multiple common regions in language and nonlanguage subnetworks

We examined the co-occurrence of nodes within subnetworks in both the whole patient group and the right-handed group (see Supplementary Tables 9 and 10). For language tasks, the left olfactory cortex and the left globe pallidum that occurred in five language tasks might be multiattribute regions that process information of multiple language attributes. For nonlanguage tasks, we found the left thalamus and the left supplementary motor area (SMA) in four tasks.

Our language findings imply that the olfactory cortex–limbic system–basal ganglia circuit may play a vital role in language processing. The limbic system comprises (i) the cingulate and hippocampal gyrus, (ii) the surrounding olfactory fibers, and (iii) the hypothalamus and amygdala (Isaacson 1982); the basal ganglia include the caudate nucleus, putamen, pallidum, and other subregions (Graybiel 2000), and these three areas in this circuit are closely related to each other (Hikosaka et al. 2008; Isaacson 1982; Tanik et al. 2016). In language function, the limbic system was thought to be involved in first and second language acquisition (Maftoon et al. 2014), and the basal ganglia was thought to be involved in spoken and sign language, syntax, and language dysfunction (Crosson 1985; Graybiel 2000; Newman et al. 2010; Zenon and Olivier 2014; Nadeau 2021). These regions, both having nonlanguage (such as the motor control and sensory information transfer) and language function, were mentioned to be the neuronal recycling hypothesis (Dehaene and Cohen 2007). Therefore, we thought that the olfactory cortex, which had a close connection with the limbic system and the basal ganglia, might have evolved the language function over the nonlanguage function.

Several studies have discovered activation of the olfactory cortex in response to words and sentences containing olfactory information (González et al. 2006; Pomp et al. 2018). For example, reading odor-related words activated the olfactory brain region compared with neutral words, and metaphorical and literal olfactory sentences recruited the secondary olfactory cortex compared with nonsmell sentences (González et al. 2006; Pomp et al. 2018). However, these results were compared by smelly and other words/sentences. They did not compare words to the chessboard, nonword string, or other low-cognitive baseline stimuli in the olfactory cortex. We hypothesized that the olfactory cortex might be more strongly activated by words (activation more in smelly words than other words) than the chessboard or nonword string. Our common language results for the olfactory cortex might have two explanations. First, our language processing tasks might engage olfactory information in these words and sentences, implying that the olfactory cortex processes both explicit and implicit olfactory information. For example, the smell of "rose" was explicit (the perfume) and that of "tiger" was implicit (the furry). Second, it is possible that the olfactory cortex serves a broader role beyond olfactory processing and may function as an information transfer hub, even for multiple nonlanguage attributes, as we observed nonlanguage effects in three attributes.

The lenticular nucleus pallidum, a part of basal ganglia which was also named the globus pallidus, might be a specific node in language processing rather than nonlanguage in our results. Previous studies mentioned that the basal ganglia had a contribution not only to motor functions but also to language processing (Crosson 1985; Liu et al. 2010; Zenon and Olivier 2014). Specifically, the globus pallidus contributed to reading ability, the second language, and its lesion might lead to language disorder in Parkinson's and Huntington's disease (Crosson 1985; Chenery et al. 2002; Liu et al. 2010; Kujala et al. 2021). Our findings indicated that the globus pallidus was involved in processing multiple language attribute information, with no observed effects in nonlanguage processing. Therefore, it might function as a comprehensive hub-like region that processed various aspects of language components, including syntactic encoding, semantic access, and attribute information management, rather than being specific to object recognition and selection.

The thalamus, typically considered a relay center for transferring sensory and motor information between subcortical or cortical sources and the cortex (Herrero et al. 2002; Sherman 2007), has been identified as important in language processing in previous studies (Wahl et al. 2008;Crosson 2013 ; Llano 2013). However, our results did not reveal a specific language effect in the thalamus. This discrepancy could be due to several reasons: (i) the thalamic lesion was a rapid recovery course from language deficits, while our patients suffered from a first-time brain injury at least 1 month postonset (this reason can be explored in some regions that we did not found in language processing); (ii) the thalamus might be more specific to naming, a more lexical-level language processing, which could not be completely explored in our comprehensive language tasks (Crosson 2013; Llano 2013).

The SMA, a part of the supplementary motor complex, contributed to self-initiated and externally triggered movements, movement sequences, behavior planning and execution, learning, and cognitive control (Alario et al. 2006; Nachev et al. 2008). In language function, the SMA was mentioned to play a role in word production (Alario et al. 2006). We found the SMA effect in four nonlanguage attributes and two language attributes (motion and sound), which meant that this region had both language and nonlanguage functions.

In our language and nonlanguage processing, we did not observe a multiattribute effect in the ATL region. Several potential reasons could explain this: (i) the lesions in patients were slightly in the temporal lobe (see Fig. 2); (ii) the ATL region might serve as a higher level region that our specific attribute tasks could not effectively measure; and (iii) low-level lesions could cut off the connections between ATL and other regions.

The investigate for previous neurocomputational model

The results of the 99-patient group strongly supported that language processing was left-lateral in the brain. For hemispheric-injury subgroups, patients with bilateral lesions exhibited left-lateralized subnetworks across all six attributes (LIs: 0.78–1); patients with left hemisphere lesions demonstrated bilateral or right-lateralized subnetworks (LIs in all 6 attributes except for color: −0.66–0), while patients with right hemisphere lesions displayed bilateral or left-lateralized subnetworks (LIs in all 6 except for sound: 0–1). Our results strongly support the predictions of this neurocomputational model (Chang and Lambon Ralph 2020).

These results might indicate that different hemispheric damage could affect language lateralization. In cases where the right hemisphere was severely damaged, the left hemisphere might compensate to restore the lost language function. In situations of severe damage in the left hemisphere, the right hemisphere may not possess sufficient capacity to fully restore the lost language function (Chang and Lambon Ralph 2020). We additionally observed that when both hemispheres were damaged, the left hemisphere was more severely impaired in language computational capacity than the right hemisphere, and the subnetwork preferentially included the left brain regions in the language network. In the hemispheric injury subgroups, the left damage subnetwork contained more nodes than the right damage subnetwork, suggesting a relatively weaker language processing capacity in the right hemisphere. When the right hemisphere was damaged, only a small amount of regions in the left hemisphere was needed for language recovery. However, when the left hemisphere was damaged, more regions were needed to restore the language function. When both hemispheres were damaged, the language network results were left-lateral because the left hemisphere was more important and had more computational capacity than

the right in language function. When the three groups were grouped, the language contribution of the right hemisphere might be hidden under the left regions of the brain because the right hemisphere had less language processing capacity (Chang and Lambon Ralph 2020).

Limitations

This study has at least the following limitations. (i) The global efficiency of these optimal subnetworks in attributes only accounted for a part of the variation in behavioral performance (R^2 range: 24%–46%). Specifically, the reasons might be: (a) damage to gray matter, which was not taken into account in our study (Bendfeldt et al. 2009); (b) recovery compensation from the acute period to the stable period (Llano 2013; Chang and Lambon Ralph 2020); (c) segmentation of node brain regions in the AAL template in which the AAL regions may have different functional subregions (Li et al. 2013; Xu et al. 2015), and these were not considered in our analysis; (d) the global efficiency measure which may not be highly sensitive enough to accurately assess the processing ability of the subnetworks under investigation; (e) the approximation of GA in the NLSM procedure where the algorithm only approximately but not exhaustively search all the candidate subnetworks; and (f) practice effect and fatigue effect of the subjects (Forbach et al. 1974). Lasty, there could be other factors stemming from the subjects themselves (e.g. low vision), the examiners (e.g. expectation effect), the testing environment (e.g. noise), and the testing machine (e.g. stimuli clearness). (ii) Some brain regions did not appear in the identified subnetworks because they had fewer patients with lesions (e.g. left and right SPG, PCG, ORPsupmed, see Supplementary Table 3). (iii) The item numbers of some attribute tasks were different, which might have confounded the differences among the attribute networks. (iv) Due to methodological limitations, we adopted GA to reduce the computational load. The obtained optimal subnetworks might not be truly optimal. (v) Some obtained attribute networks also had few nodes and edges with LIs that might not be sensitive. (vi) Our study did not examine the lateralization of the language network in all non–right-handed patients. These issues need to be explored in future studies.

Conclusion

Using the NLSM method and 99 patients with brain injuries, we constructed networks underlying the six attributes in language processes for the whole group and different subgroups to investigate the neurocomputational model (Chang and Lambon Ralph 2020). We found that networks for language processing for all six attributes were left-lateralized, while nonlanguage networks had different lateralization patterns. Regarding the language subnetworks in different lesion subgroups, lesions in one hemisphere could be compensated by another hemisphere, while the bi-lesion subgroup showed the left hemisphere language dominance. These findings reveal the importance and necessity of the left hemisphere in various language processes and support the unified and comprehensive neurocomputational model in healthy and patient individuals.

Acknowledgments

We would like to thank the members of the BNU-CNLab for their contributions to the data collection.

CRediT statement

Zhiyun Dai (Conceptualization, Data curation, Formal analysis, Visualization, Writing – original draft, Writing – review & editing), Luping Song (Data curation, Investigation, Project administration), Chongjing Luo (Data curation, Formal analysis, Visualization, Writing – original draft), Di Liu (Data curation, Formal analysis Mingyang Li Data curation, Methodology) Zaizhu Han (Conceptualization, Funding acquisition, Writing – original draft, Writing – review & editing)

Supplementary material

Supplementary material is available at *Cerebral Cortex* online.

Funding

This work was supported by the National Natural Science Foundation of China (32271091, 81972144, 81870833 and 82372555).

Conflict of interest statement: The authors declared no conflicts of interest.

Data availability

The data sets generated or analyzed during this study are available from the corresponding author on reasonable request.

References

Abbott DF, Waites AB, Lillywhite LM, Jackson GD. fMRI assessment of language lateralization: an objective approach. *NeuroImage*. 2010:50:1446–1455.

Alario F-X, Chainay H, Lehericy S, Cohen L. The role of the supplementary motor area (SMA) in word production. *Brain Res*. 2006:1076:129–143.

Arora J, Pugh K, Westerveld M, Spencer S, Spencer DD, Todd CR. Language lateralization in epilepsy patients: fMRI validated with the Wada procedure. *Epilepsia*. 2009:50:2225–2241.

Attwell D, Laughlin SB. An energy budget for signaling in the grey matter of the brain. *J Cereb Blood Flow Metab*. 2001:21:1133–1145.

Babcock LE, Robison RA. Preferences of Palaeozoic predators. *Nature*. 1989:337:695–696.

Bain JS, Yeatman JD, Schurr R, Rokem A, Mezer AA. Evaluating arcuate fasciculus laterality measurements across dataset and tractography pipelines. *Hum Brain Mapp*. 2019:40:3695–3711.

Baxendale S, Thompson PJ, Duncan JS. The role of the Wada test in the surgical treatment of temporal lobe epilepsy: an international survey. *Epilepsia*. 2008:49:715–720.

Bendfeldt K, Kuster P, Traud S, Egger H, Winklhofer S, Mueller-Lenke N, Naegelin Y, Gass A, Kappos L, Matthews PM, et al. Association of regional gray matter volume loss and progression of white matter lesions in multiple sclerosis—a longitudinal voxel-based morphometry study. *NeuroImage*. 2009:45:60–67.

Benjamini Y, Hochberg Y. Controlling the false discovery rate: a practical and powerful approach to multiple testing. *J R Stat Soc Ser B Methodol*. 1995:57:289–300.

Benjamini Y, Yekutieli D. The control of the false discovery rate in multiple testing under dependency. *Ann Stat*. 2001:29:1165–1188.

Benjamini Y, Yekutieli D. False discovery rate–adjusted multiple confidence intervals for selected parameters. *J Am Stat Assoc*. 2005:100:71–81.

Binder JR, Frost JA, Hammeke TA, Bellgowan PSF, Springer JA, Kaufman JN, Possing ET. Human temporal lobe activation by speech and nonspeech sounds. *Cereb Cortex*. 2000:10:512–528.

Binder JR, Desai RH, Graves WW, Conant LL. Where is the semantic system? A critical review and meta-analysis of 120 functional neuroimaging studies. *Cereb Cortex*. 2009:19:2767–2796.

Boronat CB, Buxbaum LJ, Coslett HB, Tang K, Saffran EM, Kimberg DY, Detre JA. Distinctions between manipulation and function knowledge of objects: evidence from functional magnetic resonance imaging. *Cogn Brain Res*. 2005:23:361–373.

Bouchard HC, Sun D, Dennis EL, Newsome MR, Disner SG, Elman J, Silva A, Velez C, Irimia A, Davenport ND, et al. Age-dependent white matter disruptions after military traumatic brain injury: multivariate analysis results from ENIGMA brain injury. *Hum Brain Mapp*. 2022:43:2653–2667.

Braet W, Humphreys GW. Case mixing and the right parietal cortex: evidence from rTMS. *Exp Brain Res*. 2006:168:265–271.

Bridge H, Thomas OM, Minini L, Cavina-Pratesi C, Milner AD, Parker AJ. Structural and functional changes across the visual cortex of a patient with visual form agnosia. *J Neurosci*. 2013:33:12779–12791.

Briellmann RS, Labate A, Harvey AS, Saling MM, Sveller C, Lillywhite L, Abbott DF, Jackson GD. Is language lateralization in temporal lobe epilepsy patients related to the nature of the epileptogenic lesion? *Epilepsia*. 2006:47:916–920.

Bright P, Moss H, Tyler LK. Unitary vs multiple semantics: PET studies of word and picture processing. *Brain Lang*. 2004:89:417–432.

Broca P. Perte de la parole, ramolissement chronique et destruction partielle du lobe antérieur gauche du cerveau. *Bull Société Anthropol Paris*. 1861:2:235–238.

Butler CR, Brambati SM, Miller BL, Gorno-Tempini M-L. The neural correlates of verbal and non-verbal semantic processing deficits in neurodegenerative disease. *Cogn Behav Neurol Off J Soc Behav Cogn Neurol*. 2009:22:73–80.

Buxbaum LJ, Saffran EM. Knowledge of object manipulation and object function: dissociations in apraxic and nonapraxic subjects. *Brain Lang*. 2002:82:179–199.

Caramazza A, Shelton JR. Domain-specific knowledge systems in the brain: the animate-inanimate distinction. *J Cogn Neurosci*. 1998:10:1–34.

Catani M, Allin MPG, Husain M, Pugliese L, Mesulam MM, Murray RM, Jones DK. Symmetries in human brain language pathways correlate with verbal recall. *Proc Natl Acad Sci U S A*. 2007:104:17163.

Chai T, Draxler RR. Root mean square error (RMSE) or mean absolute error (MAE)? – arguments against avoiding RMSE in the literature. *Geosci Model Dev*. 2014:7:1247–1250.

Chang Y-N, Lambon Ralph MA. A unified neurocomputational bilateral model of spoken language production in healthy participants and recovery in poststroke aphasia. *Proc Natl Acad Sci U S A*. 2020:117:32779–32790.

Chen Y, Chen K, Ding J, Zhang Y, Yang Q, Lv Y, Guo Q, Han Z. Neural substrates of amodal and modality-specific semantic processing within the temporal lobe: a lesion-behavior mapping study of semantic dementia. *Cortex*. 2019:120:78–91.

Chen Y, Huang L, Chen K, Ding J, Zhang Y, Yang Q, Lv Y, Han Z, Guo Q. White matter basis for the hub-and-spoke semantic representation: evidence from semantic dementia. *Brain*. 2020:143:1206–1219.

Chenery HJ, Copland DA, Murdoch BE. Complex language functions and subcortical mechanisms: evidence from Huntington's disease and patients with non-thalamic subcortical lesions. *Int J Lang Commun Disord*. 2002:37:459–474.

Cogan GB, Thesen T, Carlson C, Doyle W, Devinsky O, Pesaran B. Sensory–motor transformations for speech occur bilaterally. *Nature*. 2014:507:94–98.

Corballis MC. The evolution of lateralized brain circuits. *Front Psychol*. 2017:8:1021.

Crawford JR, Garthwaite PH. Comparing patients' predicted test scores from a regression equation with their obtained scores: a significance test and point estimate of abnormality with accompanying confidence limits. *Neuropsychology*. 2006:20:259–271.

Crosson B. Subcortical functions in language: a working model. *Brain Lang*. 1985:25:257–292.

Crosson B. Thalamic mechanisms in language: a reconsideration based on recent findings and concepts. *Brain Lang*. 2013:126:73–88.

Crow TJ, Crow LR, Done DJ, Leask S. Relative hand skill predicts academic ability: global deficits at the point of hemispheric indecision. *Neuropsychologia*. 1998:36:1275–1282.

Cui Z, Zhong S, Xu P, He Y, Gong G. PANDA: a pipeline toolbox for analyzing brain diffusion images. *Front Hum Neurosci*. 2013:7:42.

Cutting LE, Clements AM, Courtney S, Rimrodt SL, Schafer JGB, Bisesi J, Pekar JJ, Pugh KR. Differential components of sentence comprehension: beyond single word reading and memory. *NeuroImage*. 2006:29:429–438.

Dehaene S, Cohen L. Cultural recycling of cortical maps. *Neuron*. 2007:56:384–398.

Dehaene-Lambertz G, Dehaene S, Hertz-Pannier L. Functional neuroimaging of speech perception in infants. *Science*. 2003:298:2013–2015.

Dick F, Saygin AP, Galati G, Pitzalis S, Bentrovato S, D'Amico S, Wilson S, Bates E, Pizzamiglio L. What is involved and what is necessary for complex linguistic and nonlinguistic auditory processing: evidence from functional magnetic resonance imaging and lesion data. *J Cogn Neurosci*. 2007:19:799–816.

Ellmore TM, Beauchamp MS, Breier JI, Slater JD, Kalamangalam GP, O'Neill TJ, Disano MA, Tandon N. Temporal lobe white matter asymmetry and language laterality in epilepsy patients. *NeuroImage*. 2010:49:2033–2044.

Fernandino L, Binder JR, Desai RH, Pendl SL, Humphries CJ, Gross WL, Conant LL, Seidenberg MS. Concept representation reflects multimodal abstraction: a framework for embodied semantics. *Cereb Cortex*. 2016:26:2018–2034.

Fernandino L, Humphries CJ, Conant LL, Seidenberg MS, Binder JR. Heteromodal cortical areas encode sensory-motor features of word meaning. *J Neurosci*. 2016:36:9763–9769.

Floel A, Poeppel D, Buffalo EA, Braun A, Wu CW-H, Seo H-J, Stefan K, Knecht S, Cohen LG. Prefrontal cortex asymmetry for memory encoding of words and abstract shapes. *Cereb Cortex*. 2004:14:404–409.

Forbach GB, Stanners RF, Hochhaus L. Repetition and practice effects in a lexical decision task. *Mem Cogn*. 1974:2:337–339.

Forster KI, Forster JC. DMDX: a windows display program with millisecond accuracy. *Behav Res Methods Instrum Comput*. 2003:35:116–124.

Frost JA, Binder JR, Springer JA, Hammeke TA, Bellgowan PSF, Rao SM, Cox RW. Language processing is strongly left lateralized in both sexes: evidence from functional MRI. *Brain*. 1999:122:199–208.

Fujii T, Fukatsu R, Watabe S, Ohnuma A, Teramura K, Kimura I, Saso S, Kogure K. Auditory sound agnosia without aphasia following a right temporal lobe lesion. *Cortex*. 1990:26:263–268.

Gainotti G. Is the difference between right and left ATLs due to the distinction between general and social cognition or between

verbal and non-verbal representations? *Neurosci Biobehav Rev*. 2015:51:296–312.
Gajardo-Vidal A, Lorca-Puls DL, Hope TMH, Parker Jones O, Seghier ML, Prejawa S, Crinion JT, Leff AP, Green DW, Price CJ. How right hemisphere damage after stroke can impair speech comprehension. *Brain*. 2018:141:3389–3404.
Giljov A, Karenina K, Malashichev Y. Does bipedality predict the group-level manual laterality in mammals? *PLoS One*. 2012:7:e51583.
Gleichgerrcht E, Fridriksson J, Rorden C, Bonilha L. Connectome-based lesion-symptom mapping (CLSM): a novel approach to map neurological function. *NeuroImage Clin*. 2017:16:461–467.
Gleissner U, Helmstaedter C, Elger C. Right hippocampal contribution to visual memory: a presurgical and postsurgical study in patients with temporal lobe epilepsy. *J Neurol Neurosurg Psychiatry*. 1998:65:665–669.
Goebel R. BrainVoyager — past, present, future. *NeuroImage*. 2012:62:748–756.
Goldberg DE. Genetic algorithms in search, optimization and machine learning. 1st ed. USA: Addison-Wesley Longman Publishing Co., Inc. 1989.
González J, Barros-Loscertales A, Pulvermüller F, Meseguer V, Sanjuán A, Belloch V, Ávila C. Reading cinnamon activates olfactory brain regions. *NeuroImage*. 2006:32:906–912.
Graybiel AM. The basal ganglia. *Curr Biol*. 2000:10:R509–R511.
Griffis JC, Metcalf NV, Corbetta M, Shulman GL. Damage to the shortest structural paths between brain regions is associated with disruptions of resting-state functional connectivity after stroke. *NeuroImage*. 2020:210:116589.
Güntürkün O, Ströckens F, Ocklenburg S. Brain lateralization: a comparative perspective. *Physiol Rev*. 2020:100:1019–1063.
Han Z, Ma Y, Gong G, He Y, Caramazza A, Bi Y. White matter structural connectivity underlying semantic processing: evidence from brain damaged patients. *Brain*. 2013:136:2952–2965.
Hartwigsen G, Siebner HR. Probing the involvement of the right hemisphere in language processing with online transcranial magnetic stimulation in healthy volunteers. *Aphasiology*. 2012:26:1131–1152.
Herbet G, Moritz-Gasser S, Duffau H. Electrical stimulation of the dorsolateral prefrontal cortex impairs semantic cognition. *Neurology*. 2018:90:e1077–e1084.
Herrero M-T, Barcia C, Navarro J. Functional anatomy of thalamus and basal ganglia. *Childs Nerv Syst*. 2002:18:386–404.
Hikosaka O, Sesack SR, Lecourtier L, Shepard PD. Habenula: crossroad between the basal ganglia and the limbic system. *J Neurosci*. 2008:28:11825–11829.
Hoffman P, Lambon Ralph MA. Shapes, scents and sounds: quantifying the full multi-sensory basis of conceptual knowledge. *Neuropsychologia*. 2013:51:14–25.
Isaacs KL, Barr WB, Nelson PK, Devinsky O. Degree of handedness and cerebral dominance. *Neurology*. 2006:66:1855–1858.
Isaacson RL. The limbic system. Boston, MA: Springer US. 1982.
Iturria-Medina Y, Pérez Fernández A, Morris DM, Canales-Rodríguez EJ, Haroon HA, García Pentón L, Augath M, Galán García L, Logothetis N, Parker GJM, et al. Brain hemispheric structural efficiency and interconnectivity rightward asymmetry in human and nonhuman primates. *Cereb Cortex*. 2011:21:56–67.
James TW, Gauthier I. Brain areas engaged during visual judgments by involuntary access to novel semantic information. *Vis Res*. 2004:44:429–439.
James JS, Kumari SR, Sreedharan RM, Thomas B, Radhkrishnan A, Kesavadas C. Analyzing functional, structural, and anatomical correlation of hemispheric language lateralization in healthy subjects using functional MRI, diffusion tensor imaging, and voxel-based morphometry. *Neurol India*. 2015:63:49.
Janecek JK, Swanson SJ, Sabsevitz DS, Hammeke TA, Raghavan M, E. Rozman M, Binder JR. Language lateralization by fMRI and Wada testing in 229 patients with epilepsy: rates and predictors of discordance. *Epilepsia*. 2013:54:314–322.
Jones SE, Mahmoud SY, Phillips MD. A practical clinical method to quantify language lateralization in fMRI using whole-brain analysis. *NeuroImage*. 2011:54:2937–2949.
Karnath H-O, Rüter J, Mandler A, Himmelbach M. The anatomy of object recognition—visual form agnosia caused by medial occipitotemporal stroke. *J Neurosci*. 2009:29:5854–5862.
Knecht S, Deppe M, Dräger B, Bobe L, Lohmann H, Ringelstein E-B, Henningsen H. Language lateralization in healthy right-handers. *Brain*. 2000:123:74–81.
Kuhn HW. The Hungarian method for the assignment problem. *Nav Res Logist Q*. 1955:2:83–97.
Kuhnke P, Kiefer M, Hartwigsen G. Task-dependent recruitment of modality-specific and multimodal regions during conceptual processing. *Cereb Cortex*. 2020:30:3938–3959.
Kujala T, Sihvonen AJ, Thiede A, Palo-oja P, Virtala P, Numminen J, Laasonen M. Voxel and surface based whole brain analysis shows reading skill associated grey matter abnormalities in dyslexia. *Sci Rep*. 2021:11:10862.
Lambon Ralph MA, Jefferies E, Patterson K, Rogers TT. The neural and computational bases of semantic cognition. *Nat Rev Neurosci*. 2017:18:42–55.
Lange T, Roth V, Braun ML, Buhmann JM. Stability-based validation of clustering solutions. *Neural Comput*. 2004:16:1299–1323.
Latora V, Marchiori M. Efficient behavior of small-world networks. *Phys Rev Lett*. 2001:87:198701.
Lesourd M, Servant M, Baumard J, Reynaud E, Ecochard C, Medjaoui FT, Bartolo A, Osiurak F. Semantic and action tool knowledge in the brain: identifying common and distinct networks. *Neuropsychologia*. 2021:159:107918.
Li W, Qin W, Liu H, Fan L, Wang J, Jiang T, Yu C. Subregions of the human superior frontal gyrus and their connections. *NeuroImage*. 2013:78:46–58.
Li D, Tang W, Yan T, Zhang N, Xiang J, Niu Y, Wang B. Abnormalities in hemispheric lateralization of intra- and inter-hemispheric white matter connections in schizophrenia. *Brain Imaging Behav*. 2021:15:819–832.
Li M, Song L, Zhang Y, Han Z. White matter network of oral word reading identified by network-based lesion-symptom mapping. *iScience*. 2021:24:102862.
Lin L, Xue Y, Duan Q, Sun B, Lin H, Chen X, Luo L, Wei X, Zhang Z. Microstructural white matter abnormalities and cognitive dysfunction in subcortical ischemic vascular disease: an atlas-based diffusion tensor analysis study. *J Mol Neurosci*. 2015:56:363–370.
Lindell AK. In your right mind: right hemisphere contributions to language processing and production. *Neuropsychol Rev*. 2006:16:131–148.
Liu H, Hu Z, Guo T, Peng D. Speaking words in two languages with one brain: neural overlap and dissociation. *Brain Res*. 2010:1316:75–82.
Llano DA. Functional imaging of the thalamus in language. *Brain Lang*. 2013:126:62–72.
Maftoon P, Shakouri N, Nazari O. Limbic system and second language acquisition: reconsidering the role of emotion. *Biol Forum- Int J*. 2014:6:398–403.
Mesulam M-M, Wieneke C, Hurley R, Rademaker A, Thompson CK, Weintraub S, Rogalski EJ. Words and objects at the tip of the left

temporal lobe in primary progressive aphasia. *Brain*. 2013:136: 601–618.
Miceli G, Fouch E, Capasso R, Shelton JR, Tomaiuolo F, Caramazza A. The dissociation of color from form and function knowledge. *Nat Neurosci*. 2001:4:662–667.
Nachev P, Kennard C, Husain M. Functional role of the supplementary and pre-supplementary motor areas. *Nat Rev Neurosci*. 2008:9:856–869.
Nadeau SE. Basal ganglia and thalamic contributions to language function: insights from a parallel distributed processing perspective. *Neuropsychol Rev*. 2021:31:495–515.
Newman AJ, Supalla T, Hauser PC, Newport EL, Bavelier D. Prosodic and narrative processing in American sign language: an fMRI study. *NeuroImage*. 2010:52:669–676.
Ocklenburg S, Ströckens F, Güntürkün O. Lateralisation of conspecific vocalisation in non-human vertebrates. *Laterality*. 2013:18: 1–31.
Ocklenburg S, Westerhausen R, Hirnstein M, Hugdahl K. Auditory hallucinations and reduced language lateralization in schizophrenia: a meta-analysis of dichotic listening studies. *J Int Neuropsychol Soc*. 2013:19:410–418.
Ocklenburg S, Beste C, Arning L, Peterburs J, Güntürkün O. The ontogenesis of language lateralization and its relation to handedness. *Neurosci Biobehav Rev*. 2014:43:191–198.
Ocklenburg S, Güntürkün O, Hugdahl K, Hirnstein M. Laterality and mental disorders in the postgenomic age – a closer look at schizophrenia and language lateralization. *Neurosci Biobehav Rev*. 2015:59:100–110.
Oishi K, Faria A, Jiang H, Li X, Akhter K, Zhang J, Hsu JT, Miller MI, van Zijl PCM, Albert M, et al. Atlas-based whole brain white matter analysis using large deformation diffeomorphic metric mapping: application to normal elderly and Alzheimer's disease participants. *NeuroImage*. 2009:46:486–499.
Oldfield RC. The assessment and analysis of handedness: the Edinburgh inventory. *Neuropsychologia*. 1971:9:97–113.
Papagno C, Fogliata A, Catricalà E, Miniussi C. The lexical processing of abstract and concrete nouns. *Brain Res*. 2009:1263:78–86.
Parker GJM, Luzzi S, Alexander DC, Wheeler-Kingshott CAM, Ciccarelli O, Lambon Ralph MA. Lateralization of ventral and dorsal auditory-language pathways in the human brain. *NeuroImage*. 2005:24:656–666.
Partovi S, Jacobi B, Rapps N, Zipp L, Karimi S, Rengier F, Lyo JK, Stippich C. Clinical standardized fMRI reveals altered language lateralization in patients with brain tumor. *Am J Neuroradiol*. 2012:33:2151–2157.
Patterson K, Nestor PJ, Rogers TT. Where do you know what you know? The representation of semantic knowledge in the human brain. *Nat Rev Neurosci*. 2007:8:976–987.
Peeters R, Simone L, Nelissen K, Fabbri-Destro M, Vanduffel W, Rizzolatti G, Orban GA. The representation of tool use in humans and monkeys: common and uniquely human features. *J Neurosci*. 2009:29:11523–11539.
Perlaki G, Horvath R, Orsi G, Aradi M, Auer T, Varga E, Kantor G, Altbäcker A, John F, Doczi T, et al. White-matter microstructure and language lateralization in left-handers: a whole-brain MRI analysis. *Brain Cogn*. 2013:82:319–328.
Pillai JJ, Zaca D. Relative utility for hemispheric lateralization of different clinical fMRI activation tasks within a comprehensive language paradigm battery in brain tumor patients as assessed by both threshold-dependent and threshold-independent analysis methods. *NeuroImage*. 2011:54:S136–S145.
Poeppel D. The neuroanatomic and neurophysiological infrastructure for speech and language. *Curr Opin Neurobiol*. 2014:28: 142–149.
Pomp J, Bestgen A-K, Schulze P, Müller CJ, Citron FMM, Suchan B, Kuchinke L. Lexical olfaction recruits olfactory orbitofrontal cortex in metaphorical and literal contexts. *Brain Lang*. 2018:179: 11–21.
Popp M, Trumpp NM, Sim E-J, Kiefer M. Brain activation during conceptual processing of action and sound verbs. *Adv Cogn Psychol*. 2019:15:236–255.
Preti MG, Baglio F, Laganà MM, Griffanti L, Nemni R, Clerici M, Bozzali M, Baselli G. Assessing corpus callosum changes in Alzheimer's disease: comparison between tract-based spatial statistics and atlas-based tractography. *PLoS One*. 2012:7:e35856.
Price CJ, Friston KJ. Degeneracy and cognitive anatomy. *Trends Cogn Sci*. 2002:6:416–421.
Pujol J, Deus J, Losilla JM, Capdevila A. Cerebral lateralization of language in normal left-handed people studied by functional MRI. *Neurology*. 1999:52:1038.
Qi Z, Han M, Garel K, San Chen E, Gabrieli JDE. White-matter structure in the right hemisphere predicts mandarin Chinese learning success. *J Neurolinguistics, Language, Brain, and Gene: The Chinese Context*. 2015:33:14–28.
Riddoch JM, Humphreys GW. *Borb: Birmingham object recognition battery*. London: Psychology Press; 1993.
Rogers LJ. Brain lateralization and cognitive capacity. *Animals*. 2021:11:1996.
Rosazza C, Minati L, Ghielmetti F, Maccagnano E, Erbetta A, Villani F, Epifani F, Spreafico R, Bruzzone MG. Engagement of the medial temporal lobe in verbal and nonverbal memory: assessment with functional MR imaging in healthy subjects. *Am J Neuroradiol*. 2009:30:1134–1141.
Rubinov M, Sporns O. Complex network measures of brain connectivity: uses and interpretations. *NeuroImage*. 2010:52:1059–1069.
Schilling KG, Daducci A, Maier-Hein K, Poupon C, Houde J-C, Nath V, Anderson AW, Landman BA, Descoteaux M. Challenges in diffusion MRI tractography - lessons learned from international benchmark competitions. *Magn Reson Imaging*. 2019:57:194–209.
Schumacher R, Halai AD, Lambon Ralph MA. Assessing and mapping language, attention and executive multidimensional deficits in stroke aphasia. *Brain*. 2019:142:3202–3216.
Sekiyama K, Kanno I, Miura S, Sugita Y. Auditory-visual speech perception examined by fMRI and PET. *Neurosci Res*. 2003:47: 277–287.
Shaywitz BA, Shaywltz SE, Pugh KR, Constable RT, Skudlarski P, Fulbright RK, Bronen RA, Fletcher JM, Shankweiler DP, Katz L, et al. Sex differences in the functional organization of the brain for language. *Nature*. 1995:373:607–609.
Sherman SM. The thalamus is more than just a relay. *Curr Opin Neurobiol*. 2007:17:417–422.
Siniscalchi M, d'Ingeo S, Quaranta A. The dog nose "KNOWS" fear: asymmetric nostril use during sniffing at canine and human emotional stimuli. *Behav Brain Res*. 2016:304:34–41.
Siuda-Krzywicka K, Bartolomeo P. What cognitive neurology teaches us about our experience of color. *Neuroscientist*. 2020:26: 252–265.
Siuda-Krzywicka K, Witzel C, Taga M, Delanoe M, Cohen L, Bartolomeo P. When colors split from objects: the disconnection of color perception from color language and color knowledge. *Cogn Neuropsychol*. 2020:37:325–339.
Snowden JS, Thompson JC, Neary D. Knowledge of famous faces and names in semantic dementia. *Brain*. 2004:127:860–872.
Sommer IEC, Ramsey NF, Kahn RS. Language lateralization in schizophrenia, an fMRI study. *Schizophr Res*. 2001:52:57–67.
Sommer IEC, Ramsey NF, Mandl RCW, Kahn RS. Language lateralization in female patients with schizophrenia: an fMRI study. *Schizophr Res*. 2003:60:183–190.

Sotiras A, Resnick SM, Davatzikos C. Finding imaging patterns of structural covariance via non-negative matrix factorization. *NeuroImage*. 2015:108:1–16.

Sotiras A, Toledo JB, Gur RE, Gur RC, Satterthwaite TD, Davatzikos C. Patterns of coordinated cortical remodeling during adolescence and their associations with functional specialization and evolutionary expansion. *Proc Natl Acad Sci*. 2017:114:3527–3532.

Spinozzi G, Cacchiarelli B. Manual laterality in haptic and visual reaching tasks by tufted capuchin monkeys (Cebus apella). An association between hand preference and hand accuracy for food discrimination. *Neuropsychologia*. 2000:38:1685–1692.

Stasenko A, Garcea FE, Dombovy M, Mahon BZ. When concepts lose their color: a case of object-color knowledge impairment. *Cortex*. 2014:58:217–238.

Stefaniak JD, Halai AD, Lambon Ralph MA. The neural and neurocomputational bases of recovery from post-stroke aphasia. *Nat Rev Neurol*. 2020:16:43–55.

Stewart CC, Swanson SJ, Sabsevitz DS, Rozman ME, Janecek JK, Binder JR. Predictors of language lateralization in temporal lobe epilepsy. *Neuropsychologia*. 2014:60:93–102.

Ströckens F, Güntürkün O, Ocklenburg S. Limb preferences in non-human vertebrates. *Laterality*. 2013:18:536–575.

Sun Y, Chen Y, Collinson SL, Bezerianos A, Sim K. Reduced hemispheric asymmetry of brain anatomical networks is linked to schizophrenia: a connectome study. *Cereb Cortex*. 2017:27:602–615.

Sundqvist M, Routier A, Dubois B, Colliot O, Teichmann M. The white matter module-hub network of semantics revealed by semantic dementia. *J Cogn Neurosci*. 2020:32:1330–1347.

Szaflarski J, Binder J, Possing ET, McKiernan K, Ward BD, Hammeke T. Language lateralization in left-handed and ambidextrous people: fMRI data. *Neurology*. 2002:59(2):238–244.

Szaflarski JP, Holland SK, Schmithorst VJ, Byars AW. fMRI study of language lateralization in children and adults. *Hum Brain Mapp*. 2006:27:202–212.

Szaflarski JP, Rajagopal A, Altaye M, Byars AW, Jacola L, Schmithorst VJ, Schapiro MB, Plante E, Holland SK. Left-handedness and language lateralization in children. *Brain Res*. 2012:1433:85–97.

Takahashi N, Kawamura M, Shinotou H, Hirayama K, Kaga K, Shindo M. Pure word deafness due to left hemisphere damage. *Cortex*. 1992:28:295–303.

Tanik N, Serin HI, Celikbilek A, Inan LE, Gundogdu F. Associations of olfactory bulb and depth of olfactory sulcus with basal ganglia and hippocampus in patients with Parkinson's disease. *Neurosci Lett*. 2016:620:111–114.

Thierry G, Price CJ. Dissociating verbal and nonverbal conceptual processing in the human brain. *J Cogn Neurosci*. 2006:18:1018–1028.

Thierry G, Giraud A-L, Price C. Hemispheric dissociation in access to the human semantic system. *Neuron*. 2003:38:499–506.

Tustison NJ, Cook PA, Klein A, Song G, Das SR, Duda JT, Kandel BM, van Strien N, Stone JR, Gee JC, et al. Large-scale evaluation of ANTs and FreeSurfer cortical thickness measurements. *NeuroImage*. 2014:99:166–179.

Tzourio-Mazoyer N, Landeau B, Papathanassiou D, Crivello F, Etard O, Delcroix N, Mazoyer B, Joliot M. Automated anatomical labeling of activations in SPM using a macroscopic anatomical parcellation of the MNI MRI single-subject brain. *NeuroImage*. 2002:15:273–289.

van Kooij BJM, de Vries LS, Ball G, van Haastert IC, Benders MJNL, Groenendaal F, Counsell SJ. Neonatal tract-based spatial statistics findings and outcome in preterm infants. *Am J Neuroradiol*. 2012:33:188–194.

Vallortigara G, Rogers LJ. Survival with an asymmetrical brain: advantages and disadvantages of cerebral lateralization. *Behav Brain Sci*. 2005:28:575–589.

Vartanian O, Goel V. Task constraints modulate activation in right ventral lateral prefrontal cortex. *NeuroImage*. 2005:27:927–933.

Vigneau M, Beaucousin V, Hervé P-Y, Jobard G, Petit L, Crivello F, Mellet E, Zago L, Mazoyer B, Tzourio-Mazoyer N. What is right-hemisphere contribution to phonological, lexico-semantic, and sentence processing? Insights from a meta-analysis. *NeuroImage*. 2011:54:577–593.

Vinberg J, Grill-Spector K. Representation of shapes, edges, and surfaces across multiple cues in the human visual cortex. *J Neurophysiol*. 2008:99:1380–1393.

Vingerhoets G, Acke F, Alderweireldt A, Nys J, Vandemaele P, Achten E. Cerebral lateralization of praxis in right- and left-handedness: same pattern, different strength. *Hum Brain Mapp*. 2011:33:763–777.

Wahl M, Marzinzik F, Friederici AD, Hahne A, Kupsch A, Schneider G-H, Saddy D, Curio G, Klostermann F. The human thalamus processes syntactic and semantic language violations. *Neuron*. 2008:59:695–707.

Wallentin M. Putative sex differences in verbal abilities and language cortex: a critical review. *Brain Lang*. 2009:108:175–183.

Wilke M, Lidzba K. LI-tool: a new toolbox to assess lateralization in functional MR-data. *J Neurosci Methods*. 2007:163:128–136.

Xu J, Wang J, Fan L, Li H, Zhang W, Hu Q, Jiang T. Tractography-based parcellation of the human middle temporal gyrus. *Sci Rep*. 2015:5:18883.

Yamazaki Y, Aust U, Huber L, Hausmann M, Güntürkün O. Lateralized cognition: asymmetrical and complementary strategies of pigeons during discrimination of the "human concept.". *Cognition*. 2007:104:315–344.

Yeh F-C, Panesar S, Fernandes D, Meola A, Yoshino M, Fernandez-Miranda JC, Vettel JM, Verstynen T. Population-averaged atlas of the macroscale human structural connectome and its network topology. *NeuroImage*. 2018:178:57–68.

Zacà D, Nickerson JP, Deib G, Pillai JJ. Effectiveness of four different clinical fMRI paradigms for preoperative regional determination of language lateralization in patients with brain tumors. *Neuroradiology*. 2012:54:1015–1025.

Zacà D, Corsini F, Rozzanigo U, Dallabona M, Avesani P, Annicchiarico L, Zigiotto L, Faraca G, Chioffi F, Jovicich J, et al. Whole-brain network connectivity underlying the human speech articulation as emerged integrating direct electric stimulation, resting state fMRI and tractography. *Front Hum Neurosci*. 2018:12:405.

Zenon A, Olivier E. Contribution of the basal ganglia to spoken language: is speech production like the other motor skills? *Behav Brain Sci*. 2014:37:576–576.

Zhao Y, Song L, Ding J, Lin N, Wang Q, Du X, Sun R, Han Z. Left anterior temporal lobe and bilateral anterior cingulate cortex are semantic hub regions: evidence from behavior-nodal degree mapping in brain-damaged patients. *J Neurosci*. 2017:37:141–151.

Zou T-X, She L, Zhan C, Gao Y-Q, Chen H-J. Altered topological properties of gray matter structural covariance networks in minimal hepatic encephalopathy. *Front Neuroanat*. 2018:12:101.